POLITECNICO
MILANO 1863

SCUOLA DI INGEGNERIA INDUSTRIALE
E DELL'INFORMAZIONE

Optimization of polyynes production by Pulsed Laser Ablation in Liquid through a recirculation system

TESI DI LAUREA MAGISTRALE IN
MATERIALS ENGINEERING AND NANOTECHNOLOGY
INGEGNERIA DEI MATERIALI E DELLE NANOTECNOLOGIE

Author: **Federico Bertocco**

Student ID: 995633
Advisor: Carlo S. Casari
Co-advisor: Simone Melesi
Academic Year: 2023-2024

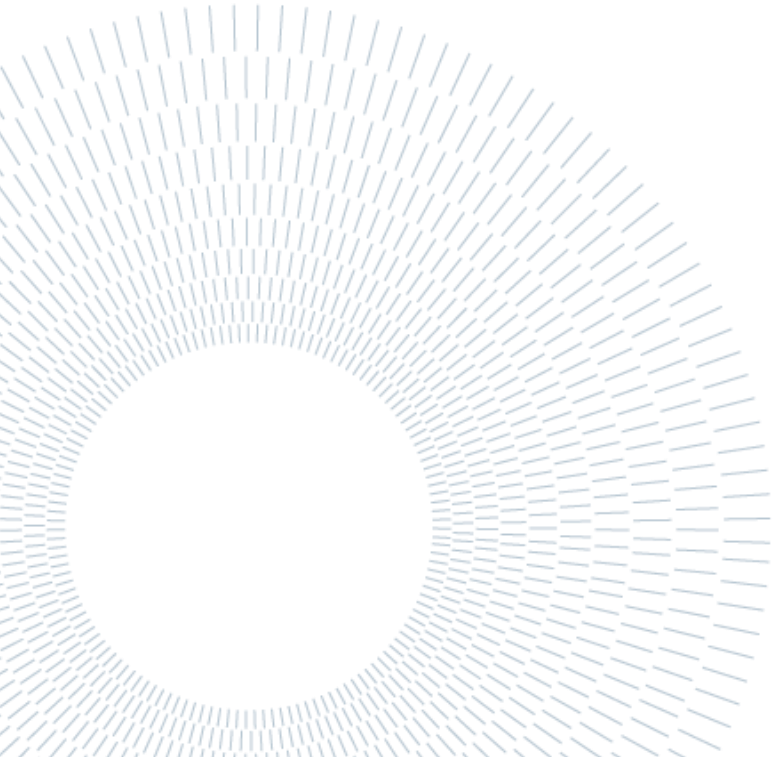

Abstract

In this thesis work, I investigated the production of polyynes by Pulsed Laser Ablation in Liquid (PLAL) through a novel recirculation method. I designed a recirculation system that allows to ablate a solid graphite target immersed in a solvent in flow conditions within an ablation cell. This flow is generated by a peristaltic membrane pump. The ablations were performed using an Nd:YAG ns-pulsed laser at the fundamental wavelength of 1064 nm. The laser ablated the graphite target for 90 minutes in the presence of 100 ml of solvent. I explored the effects of two organic solvents: methanol (MeOH) and acetonitrile (ACN). Among these, ACN was chosen for the experiments due to its higher production of polyynes (i.e., the concentration of HC_8H in ACN was twice the one in MeOH). Ablations were performed in a cell configuration where the cell volume was entirely filled by the solvent. The impact of fluence and spot radius on the final concentration of polyynes was investigated. An increase in both spot size and fluence was shown to enhance polyynes production up to a threshold, where a trend inversion occurs. For instance, the concentration of HC_8H was increased by 90% thanks to a radius increase of 24% at constant fluence. An ablation in batch (static) conditions using the same parameters of the recirculation system was performed to compare the two methods. Ablating in flow conditions, the concentration of short polyynes showed a slight increase (15% for HC_8H), while longer polyynes experienced a decrease (50% for $HC_{14}H$). The most promising result regards the rate of production, which decreased over time but with a lower gradient in the recirculation case. Indeed, in the last 15 minutes of ablation, the rate of production obtained in the recirculation system is more than 30% higher for HC_8H and approximately an order of magnitude higher for $HC_{14}H$ compared to the static case. These results show promising future perspectives for the scalability of the technique.

Key-words: Carbon atomic wires, polyynes, Pulsed Laser Ablation in Liquid, recirculation, flow, optimization.

Abstract in italiano

In questa tesi, ho indagato la produzione di poliine attraverso l'Ablazione Laser Pulsata in Liquido (PLAL) utilizzando un innovativo metodo di ricircolo. Ho progettato un sistema di ricircolo che consente di ablare un target solido di grafite immerso in un solvente in condizioni di flusso all'interno di una cella di ablazione. Questo flusso è generato da una pompa peristaltica a membrana. Le ablazioni sono state eseguite utilizzando un laser Nd:YAG ns-pulsato alla lunghezza d'onda fondamentale di 1064 nm. In ogni ablazione il target viene ablato per 90 minuti in presenza di 100 ml di solvente. Ho esplorato gli effetti di due solventi organici: metanolo (MeOH) e acetonitrile (ACN). Tra questi, l'ACN è stato scelto per gli esperimenti a causa della sua maggiore produzione di poliine, infatti la concentrazione di HC_8H in ACN è risultata circa doppia rispetto a quella in MeOH. Le ablazioni sono state eseguite con una configurazione della cella in cui il volume della cella era completamente riempito dal solvente. In tale configurazione ho investigato l'impatto della fluenza e del raggio dello spot sulla concentrazione finale di poliine. Un aumento sia delle dimensioni dello spot che della fluenza ha dimostrato di migliorare la produzione di poliine fino a una certa soglia, oltre la quale si verifica un'inversione del trend. Ad esempio, la concentrazione di HC_8H è aumentata del 90% grazie a un incremento del raggio del 24% a fluenza costante. Un' ablazione in condizioni di produzione batch (statica) è stata eseguita con gli stessi parametri utilizzati in condizioni di ricircolo per confrontare i due metodi. Ablando in condizioni di flusso, la concentrazione di poliine corte ha mostrato un lieve aumento (15% per HC_8H), mentre le poliine più lunghe hanno subito una diminuzione (50% per $HC_{14}H$). Il risultato più promettente riguarda il tasso di produzione, che diminuisce nel tempo ma con un gradiente più basso nel caso di ricircolo. Infatti, negli ultimi 15 minuti di ablazione, il tasso di produzione ottenuto nel sistema di ricircolo è superiore del 30% per HC_8H e approssimativamente di un ordine di grandezza superiore per $HC_{14}H$ rispetto al caso statico. Questi risultati suggeriscono prospettive future promettenti per uno scale-up della tecnica.

Parole chiave: Carbon atomic wires, nanofili di carbonio, ablazione pulsata in liquido, ricircolo, flusso, ottimizzazione.

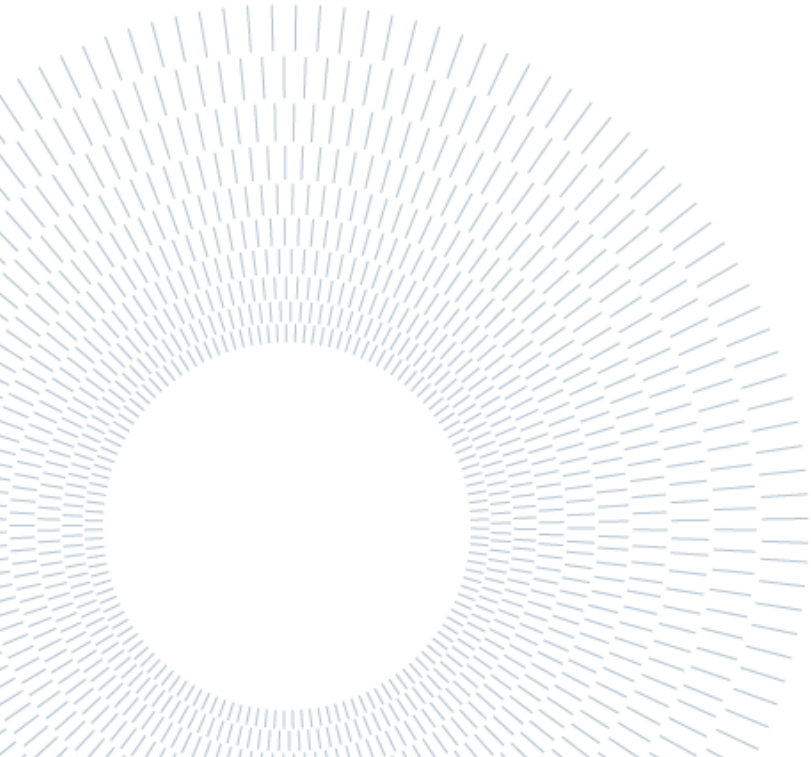

Contents

Introduction

In the field of nanotechnology, carbon-based nanostructures play a crucial role in research and technological applications. Materials like graphene, carbon nanotubes, and fullerenes exhibit exceptional properties and represent some of the most compact structures possible. The great variety of carbon-based nanostructures arises from the hybridization of carbon atoms (sp3, sp2, and sp). While solid allotropic forms of sp3 and sp2 carbon are well-established, the existence of a stable allotropic form of sp carbon remains debated. However, linear sp carbon compounds, known as Carbon Atomic Wires (CAWs), have been observed in space and synthesized using various chemical and physical methods. CAWs are the most confined 1D materials, with a diameter equivalent to a single atom. Theoretically, CAWs should exhibit remarkable properties suitable for electronics, optics, and mechanics. However, their stability poses challenges due to degradation processes like crosslinking and oxidation. The theoretical description of CAWs begins with the infinite chain model, that is an infinite linear chain of sp carbon atoms. Within this framework, two distinct structures emerge: cumulene, where carbon atoms are connected by consecutive double bonds, and polyyne, characterized by alternating single and triple bonds. In real finite CAWs, polyynes are the stable isomer for long chains due to Peierls' distortions. Shorter chains are more influenced by endgroups, which can affect the structures and properties. CAWs are mainly synthesized by two different approaches. Chemical synthesis methods produce CAWs through chemical reactions, enabling control over chain length and terminations. However, these methods are not feasible for large-scale industrial production. On the other hand, physical methods are more cost-effective and do not require complex reagents. The physical method employed in this thesis work is Pulsed Laser Ablation in Liquid (PLAL). In PLAL, a pulsed laser interacts with a target submerged in a liquid environment. The resulting out-of-equilibrium plasma promotes the formation of sp-carbon chains. Typically, hydrogen-capped polyynes are the most concentrated chains produced via PLAL. Although other terminations have been reported, achieving precise control over terminations remains challenging in PLAL synthesis.

In this work, I developed a novel recirculation system for producing polyynes via PLAL under liquid flow conditions. I investigated the effects of various parameters that influence ablation, utilizing different ablation cell configurations and adjusting

laser parameters such as fluence and spot radius. My goal was to optimize polyynes production compared to the conventional batch production method.

This work is structured as follows:

- **Chapter 1:** an overview on carbon allotropes and description of carbyne infinite model is given. Then focusing on the real finite sp-carbon chain (CAW), delving into its properties, synthesis methods and characterization methods.
- **Chapter 2:** a general description of PLAL, focusing on the physical processes involved is given. Then the state of the art of CAWs production by PLAL is presented, highlighting the possible PLAL configurations, the formation mechanisms of polyynes, and the main parameters involved.
- **Chapter 3:** the materials and experimental methods employed in this work are presented, also showing the PLAL setup for the recirculation production.
- **Chapter 4:** the experimental results obtained are presented**.** At first showing the design and possible configurations of the recirculation system. Then focusing on the optimization of the process, where the best conditions and parameters for polyynes production are described. In the last part the comparison with the results obtained in batch production is shown.

1 Carbon Atomic Wires

Carbon Atomic Wires (CAWs) are unique structures composed only of sp-hybridized carbon atoms linked together in linear chains. These wires have a diameter corresponding to a single carbon atom, making them some of the smallest and most confined structures possible [1]. They possess remarkable theoretically predicted properties such as high electrical and thermal conductivity, and an excellent mechanical strength suitable for a wide variety of applications in electronics, optics, and mechanics [1].

However, their inherent instability and ease of degradation through crosslinking, oxidation, and other processes limit their practical applications [2]. Despite these challenges, researchers continue to explore the synthesis, characterization, and potential applications of these fascinating structures thanks to their promising properties.

CAWs have been found in various natural environments such as in interstellar dust, meteorites, and they have been also isolated in some plants [3]; thus providing evidence for their existence in the universe. In 1985, Kroto and Smalley made the surprising discovery of fullerenes while studying small linear carbon chains and the formation of long-chain carbon molecules in space [4]. According to Hirsch, this coincidental discovery ignited a resurgence of interest in carbon-based nanostructures and brought to a new age of synthetic carbon allotropes [5]. Since the finding of C60 fullerene, many other carbon-based nanomaterials have been discovered and studied, such as carbon nanotubes, graphene, and more recently, Carbon Atomic Wires. The high availability of carbon in nature is another factor contributing to interest in carbon nanostructures: carbon is the fourth most abundant element in our solar system and the sixth most in the entire universe.

In this chapter, I will present a general overview on carbon allotropes particularly focused on Carbon Atomic Wires, with a general description of their properties, synthesis methods, and characterization techniques.

1.1. Overview of carbon allotropes

Carbon is a versatile element since it can arrange its valence electrons in different hybridization states producing a wide variety of allotropic forms, molecules, and

nanostructures. The presence of these structures and the chemical behaviour of carbon are explained by the hybridization theory in the framework of Linear Combination of Atomic Orbitals (LCAO). Carbon electronic configuration (i.e., $1s^2$, $2s^2$, $2p^2$) would allow it to make only two chemical bonds. However, LCAO predicts the formation of sp, sp2, and sp3 hybrid orbitals linearly combining the 2s and 2p orbitals. These orbitals and the ones that are not involved in the hybridization can be used to build single, double, and triple bonds.

In carbon-based molecules, the three possible sp3, sp2, and sp hybridizations lead to alkanes, alkenes, and alkynes molecules characterized by a tetrahedral (3-Dimensional), planar (2-Dimensional) and linear (1-Dimensional) spatial organization, respectively [6]. Considering bulk solid systems carbon shows only two possible allotropes: graphite and diamond corresponding to sp2 and sp3 hybridization respectively. As it is shown in Figure 1. 1 , the third crystalline allotropic form based on sp carbon atoms is still missing, and its existence is questionable or even considered impossible for stability reasons [2].

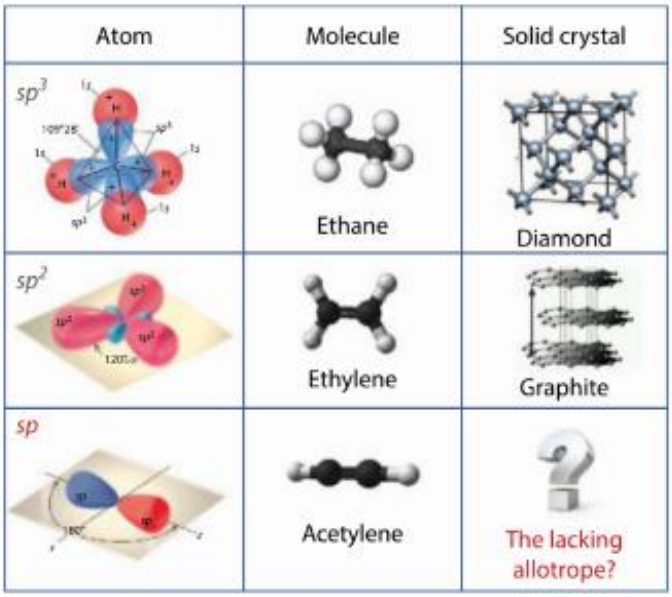

Figure 1. 1 Examples of molecules and solid crystals presenting the three possible carbon hybridization states. In red it is highlighted the missing sp-carbon allotrope [7].

For a long time, diamond and graphite were considered the only two existing carbon allotropes, but over the last decades a new class of carbon nanostructures has been discovered, demonstrating that carbon can form a wide variety of structures based on different hybridizations. These low-dimensional carbon structures are characterized by the confinement of at least one dimension to the nanometre level and they include fullerenes and nanodiamonds as quasi-zero-dimensional (quasi-0-D), nanotubes as

quasi-one-dimensional (quasi-1-D), and graphene as two-dimensional (2-D) system [1].

As shown in Figure 1. 2, carbon nanostructures can be classified according to their hybridization using a ternary diagram. The vertices are represented by structures with sp, sp2, sp3 hybridization, which correspond to molecules in the form of CAWs, graphene, and nanodiamonds, respectively. On the lines connecting the vertices, there are structures with mixed hybridization, such as graphynes and nanotubes.

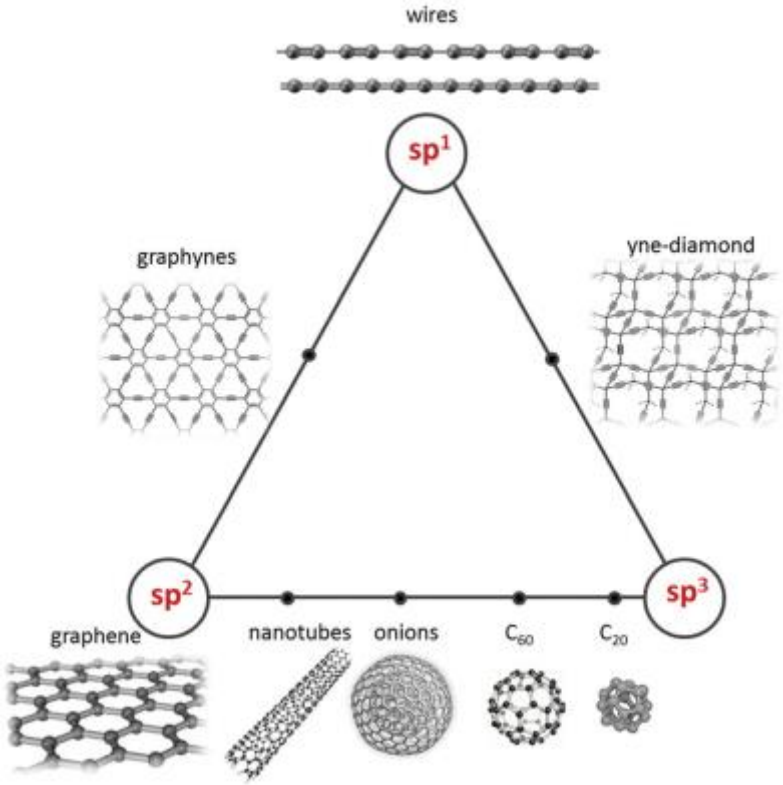

Figure 1. 2 Ternary diagram of carbon nanostructures according to their hybridization state [1].

All the structures based on sp or sp2 hybridized carbons are characterized by π-conjugation that is responsible of their outstanding electronic and optical properties, for example giving graphene and nanotubes a metallic behaviour [1]. As will be discussed in section 1.2, the ideal infinite Carbon Atomic Wire, named carbyne, can show either semiconducting or metallic properties due to the π-conjugation effect, depending on the different structures that this model can create.

1.2. The ideal model of carbyne

As mentioned above, there are many nanostructures containing sp carbon atoms, but a pure sp-hybridized carbon allotrope has not been discovered yet and its existence is still under debate [6]. This infinite linear sp-carbon chain, called carbyne, represents

the ideal model of Carbon Atomic Wires [1]. In this work 'carbyne' will be used to indicate the infinite model and the real systems made of a finite carbon chain will be referred to as Carbon Atomic Wires (CAWs).

It is worth starting the description from the ideal infinite model because it provides a theoretical basis to describe finite real systems. Due to sp-hybridizations, carbyne ideally exists in two different arrangements: one containing only double bonds, called cumulene, and the other containing an alternation of single and triple bonds, called polyyne (see Figure 1. 3) [1]. According to the LCAO theory, each sp-carbon atom in the chain combines two 2p orbitals to generate delocalized molecular orbitals giving rise to a highly conjugated molecule with delocalized π-electrons.

Cumulene has the highest conjugation due to its continuous sequence of double bonds, allowing for the delocalization of π-electrons along the whole chain. Polyyne, instead, presents a lower conjugation because of the presence of single bonds that localize more the electrons affecting its electrical properties [6]. Even if cumulene and polyyne can both be described as 1-D crystals, due to their different chemical structure, they possess different unit cells. Cumulenes contain only one carbon atom per unit cell contributing with one electron for each of the two 2p orbitals; polyynes contain two carbon atoms per unit cell contributing with two electrons per each sp2 orbitals. Thus, cumulene has a half-filled conduction band, which makes it an electrical conductor, while polyyne, is characterized by a gap at the edges of the Brillouin zone with a completely filled valence band and an empty conduction band, making it a semiconductor [1] (see Figure 1. 3).

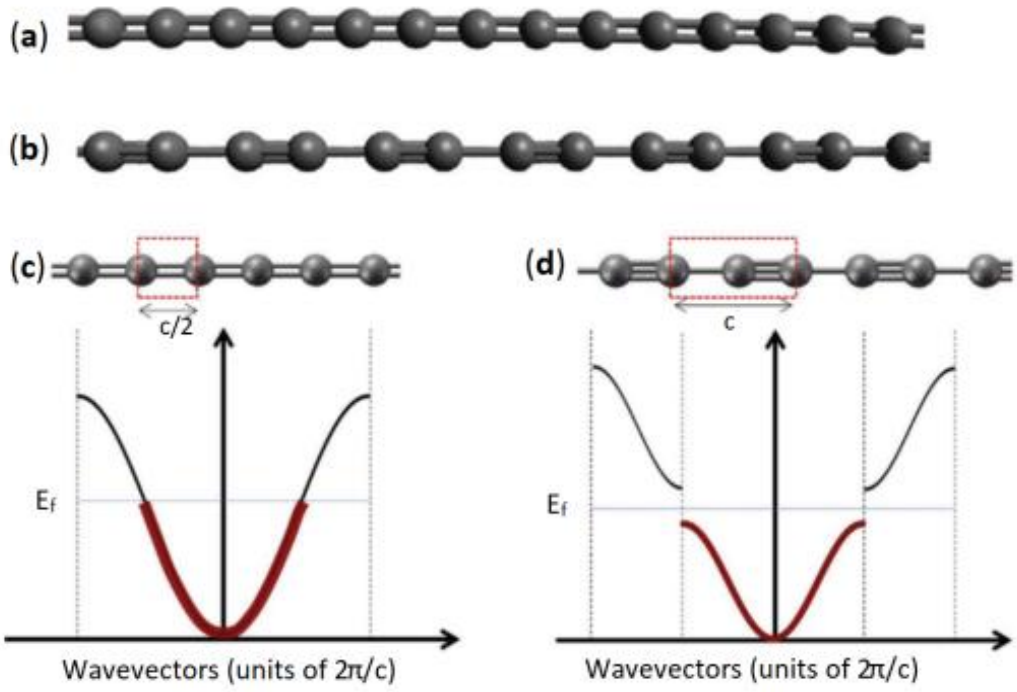

Figure 1. 3 Schematic structures of a) cumulene; b) polyyne. The electronic band structure of c) cumulene and d) polyyne. The unit cell of each isomer is highlighted in red [1].

The π-conjugation also affects the length of carbynes bonds, making shorter single bonds and longer triple bonds [6]. Since bond lengths and conjugation are linked, the Bond Length Alternation (BLA), which is the average difference between neighboring carbon bonds in a chain, is a key characteristic of carbynes [1]. The BLA is a valuable metric for examining not only the structure but also the electronic properties of sp-carbon chains. Ideal cumulenes, for instance, have a zero BLA, while ideal polyynes have a non-zero BLA.

The electronic structure of the sp-carbon chain is considerably linked to BLA. An increase in BLA corresponds to a decrease in the system's conjugation and an increase in the band gap, leading to a shift from a metallic to a semiconducting behaviour which influences both the optical and vibrational properties of the system [1]. The vibrational properties of the two isomers are also different: cumulene, having only one atom in the basis, has only the acoustic branch in the phonon dispersion relation. Polyyne, featuring two atoms per basis, shows also an optical branch [6]. As a result, cumulenes are theoretically not optically active, making ideal infinite cumulenic chains undetectable by vibrational spectroscopy.

Due to Peierls' distortion, a characteristic shared by CAWs and other polyconjugated materials like polyacetylene and polyenes, cumulene and polyyne do not have the same stability. The infinite chain structure with equal double bonds converts into a more energy-efficient dimerized chain with an alternating structure. As a result, the configuration that is more stable and has less energy is the polyynic one [1], as depicted in Figure 1. 4.

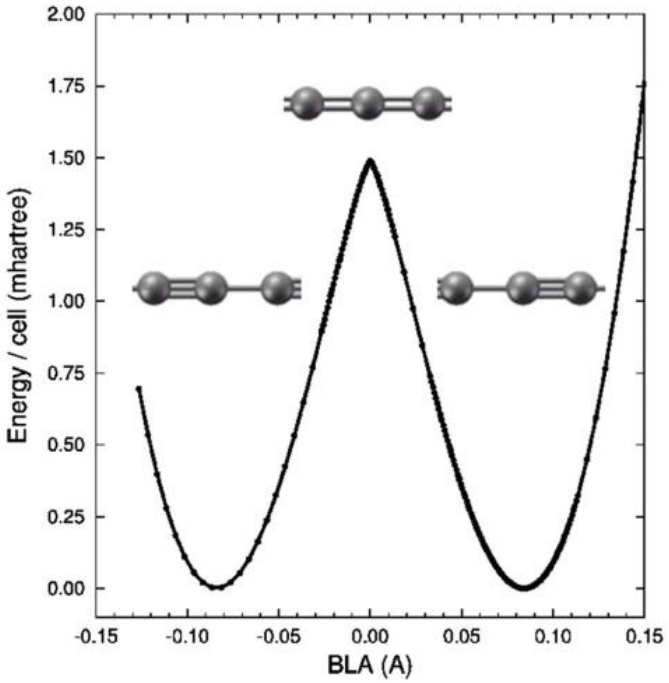

Figure 1. 4 Potential energy surface of an isolated carbyne as a function of BLA [1].

In addition to its electronic and optical characteristics, carbyne has several other notable properties. Its vibrational structure allows the phonon transport on a micron scale, leading to a high thermal conductivity (200 mK/m/K) [2], up to two orders of magnitude higher than graphene. The rigidity of the sp bonds makes carbyne suitable for mechanical applications, with a predicted elastic modulus of 32 TPa [4], surpassing that of graphene and Carbon Nanotubes (CNTs) and one of the highest ever recorded.

The ideal model of an infinite sp chain can be modified to interpret the characteristics of finite CAWs. Indeed, real systems can be correlated to the corresponding infinite chain possessing the same BLA [8], as long as the influences of their finite dimensions (e.g., the existence of terminations and the absence of infinite periodicity) are considered.

1.3. CAWs

In the previous section, it is explored the ideal model of carbyne, an infinite sp-carbon chain, and its remarkable properties. This model, while useful for understanding the inherent characteristics of carbyne, represents an idealized scenario. In reality, linear sp-carbon chains are finite, possess termination groups at their ends, and are called Carbon Atomic Wires (CAWs). These deviations from carbynes can significantly influence their properties, introducing a new layer of complexity to our understanding of this fascinating material.

1.3.1. The effect of termination groups and sp-chain lengths

Since CAWs are molecules, they cannot be described with an electronic band theory, typical of solid-state physics approach. Instead, they show discrete energy levels due to the quantum confinement caused by the finite length of the chain [1]. Their electronic and optical characteristics are related to specific energy levels such as the Highest Occupied Molecular Orbital (HOMO), that is the molecular orbital with the highest energy still occupied by electrons, and the Lowest Unoccupied Molecular Orbital (LUMO), that is the molecular orbital with the lowest energy still unoccupied [1]. The energy difference between the HOMO and the LUMO, that corresponds to the energy gap, is particularly important because it is the minimum photon energy that the molecule can absorb. This gap is affected both by the length of the chain and the termination groups, because they affect the conjugation of the molecule. Indeed, longer chains have a higher number of delocalized electrons, leading to a higher conjugation, so a smaller BLA and a smaller HOMO-LUMO gap [1], as it is shown in Figure 1. 5.

However, the limit of BLA=0, corresponding to the ideal cumulene, cannot be reached because of Peierls' distortion [8]. For CAWs, this effect has been studied to be relevant only for very long chains with more than 52 carbon atoms, where it can overcome the effect of electron delocalization on BLA [1]. For shorter chains, endgroups have a stronger influence on the structure and the vibrational and electronic properties [1].

In CAWs, therefore, the stable configuration, as well as the value of BLA, is the result of the balance between Peierls' distortion and endgroup effects, with the former dominating in longer chains, and the latter in shorter [1]. So, in real systems, the chemical nature of the terminal groups mainly determines the configuration of the sp-carbon chains, imposing a certain type of bond (i.e., single or double) to the closest carbon atom and inducing a cumulenic or polyynic structure, those affecting the electronic configuration and the properties of these systems. For example, if the endgroup forms a single bond with the first carbon, the resulting structure is a polyynic chain, but if a double bond is formed, the structure tends to be a cumulene [9].

The chemical structure of the endgroups can also influences the optical properties of the CAWs. Specifically, the endgroups modulate the BLA, affecting the HOMO-LUMO gap and the absorption spectrum [1]. Therefore, since CAWs energy gap is related to their structure, it is possible to tune their properties by just changing length and terminations.

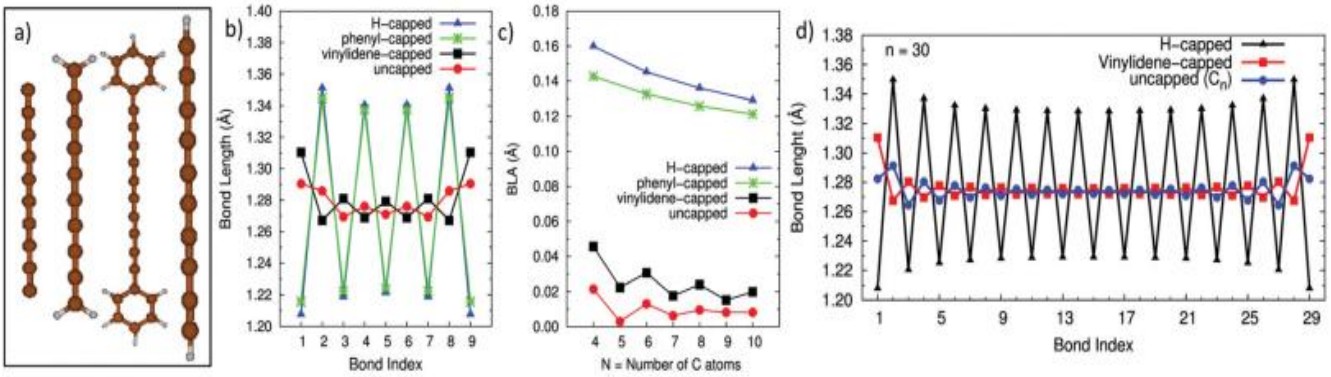

Figure 1. 5 (a) Structure of 4 different wires (from left to right): uncapped, vinylidene-, phenyl- and H-endcapped; (b and c) bond length and BLA as a function of the number of carbon atoms for different types of wires. (d) Bond lengths in long wires (i.e., 30 carbon atoms) with different terminations. Data are from DFT calculations [1].

The simplest and most common termination for polyynes is hydrogen-capping, instead for cumulenes is two hydrogen atoms [10]. Among the other endgroups, some of the most common are methyl or nitrogen [11], or bulkier endgroups, such as phenyl and biphenyl terminations [12].

1.3.2. Stability issues

Since CAWs are not naturally favoured and are formed under non-equilibrium conditions, they present a very low stability. Due to the presence of energetic π orbitals, these structures are reactive, and they tend to lose their linearity degrading into more stable sp2 structures when interacting with other chains (i.e., crosslinking and reorganization processes) [2].

Several strategies have been studied to overcome these stability issues. One approach involves tailoring the end group termination to prevent crosslinking, typically achieved with bulky termination groups that provide steric hindrance and reducing the probability of crosslinking between adjacent sp-carbon chains [12]. This principle has been successfully exploited by Tykwinski and co-workers to synthesize polyynes up to 48 atoms long [13]. Another strategy to reduce crosslinking involves embedding the chains in solid matrices, such as polymers or silica gels, to minimize interaction between CAWs. The longest CAWs ever synthesized, reaching a length of 6000 carbon atoms, were achieved by embedding it inside a nanotube [14].

In addition to crosslinking, oxidation and hydrogenation also impact the stability of CAWs [15]. Oxidation occurs due to the presence of oxidizing agents, making CAWs unstable in air. Hydrogenation is due to the highly unsaturated nature of the chains, which can bond with atomic hydrogen and break the sp-hybridization [15]. Liquids provide safer environments for sp-chains as they reduce chain-chain interactions and

oxidation [10]. Therefore, the solubility of oxygen in a solvent is a key parameter for CAWs stability.

1.4. Synthesis of CAWs

Nowadays, there are many techniques documented in the literature for the synthesis of sp-carbon wires. The different techniques are based on both physical and chemical strategies mainly in a bottom-up approach.

1.4.1. Chemical synthesis

Chemical synthesis of linear sp-carbon chains can be divided into two main categories. The first approach involves a polymerization process that starts from polymer molecules or hydrocarbon compounds, as the condensation of acetylenic units [1]. The second approach exploits the dimerization reaction of the ethynyl group from molecules with a defined length and endgroups, also called Glaser reaction [8]. The first approach can generate sp-chains in a single step, but with a wide range of lengths. On the other hand, the Glaser reaction allows to create chains with specific length and termination [8].

These methods provide a high degree of control over the process and the final products, allowing for the production of longer chains compared to physical methods, thanks to the possibility of ending the chain with bulkier stabilizing groups [10]. In literature [16], the synthesis of very long, until 68 carbon atoms, and stable chains is reported [17].

While chemical synthesis methods offer significant advantages, they also present some drawbacks. Transitioning these techniques from a laboratory setting to an industrial scale is a complex process because they are expensive, and they involve the use of toxic solvents and reagents [1]. Furthermore, these chemical processes are complex, and they need several steps to reach the final product. Each CAW needs its own process, leading to a huge number of possible chemical reactions.

1.4.2. Physical synthesis

Physical synthesis methods to produce CAWs rely on the creation of a carbon vapor or plasma, which is rapidly quenched to induce the clustering of carbon atoms under out-of-equilibrium conditions [1]. This carbon vapor or plasma can be generated through techniques such as arc discharge or laser ablation, and the quenching process is favoured using inert gas or liquids [1]. With these techniques it is easier to produce polyynes instead of cumulenes due to their higher stability.

The simplicity of the setup, faster processing time, and the ability to use safer and more eco-friendly materials such as graphite, water, and ethanol make physical methods easier than chemical synthesis to scale up for industrial production [1]. However, one

of the main drawbacks is the low control on the products, because during the process it occurs a simultaneous synthesis of many different polyynes and other carbon-based structures. Additionally, the concentration of synthesized polyynes is typically lower than that achieved with chemical methods, which can pose challenges for their characterization (e.g., Raman spectroscopy) and subsequent applications [18].

The most common physical techniques are Submerge Arc Discharge in Liquid (SADL) and Pulsed Laser Ablation in Liquid (PLAL), and they both take advantage of a liquid phase as a quenching medium for the carbon plasma [11]. The solvent is not only important for this reason but also because it may represent a secondary source of carbon and group terminations. Thus, organic solvents are favoured in these physical processes because, being sources of carbon, they can enhance the production [10].

In the SADL process, sp-carbon chains are formed by applying a high voltage to two graphite electrodes that are almost touching and submerged in a dielectric solvent, which could be water or an organic solvent. An arc discharge is produced between the two electrodes, generating a plasma region responsible of the etching of carbon atoms from graphite and atomization from the solvent, bringing to the formation of sp carbon chains [19].

In the case of PLAL, the plasma is created by a high-energy pulsed laser typically focused on a target. While graphite is a common choice for the target, other materials like polymers or metals can also be used [1]. Since the process is influenced by numerous other parameters, a more detailed explanation of the PLAL process will be provided in the following chapter.

1.5. Characterization of CAWs

Various methods can be employed to characterize CAWs. Some of the most relevant techniques are UV-Vis Spectroscopy, High-Performance Liquid Chromatography (HPLC), and Raman Spectroscopy. These techniques exploit different physical processes to characterize CAWs. UV-Vis and Raman are based on light-matter interaction, instead HPLC on material properties, such as chemical affinity with the chromatographic column and steric hindrance. UV-Vis absorption technique is employed to determine CAWs' absorption spectra, investigate their optical properties (e.g., the HOMO-LUMO gap), and assess their concentration in solutions. Raman spectroscopy allows to identify the endgroups of CAWs, since their vibrational properties are strongly linked to their structure and electronic configuration. Furthermore, High-Performance Liquid Chromatography (HPLC), exploiting physical and chemical process, can detect, separate, and collect individual CAWs species within a polydisperse solution.

1.5.1. UV-Vis absorption technique

UV-Vis spectroscopy is one of the most used techniques and it relies on the absorption of electromagnetic radiation ranging from ultraviolet to near-infrared wavelengths by the analyte under investigation [20]. When the energy of the photons matches a transition between two electronic states, they are absorbed, and electrons are excited to higher electronic states. Thus, the UV-Vis spectrophotometer by irradiating the sample reports the absorbance as a function of the incident wavelengths creating the absorption spectrum of the material itself. Each peak observed in the absorption spectrum at a specific wavelength corresponds to a distinct electronic transition of the sample. The absorption spectrum of a particular material gives information about its electronic structure, but it is worth noting that some electronic transitions might be common to different molecules.

Thanks to the Lambert-Beer law [20], UV-Vis spectroscopy provides also essential information about the concentration of the analyzed species in solution which is directly correlated to the intensity of the measured absorbance. This law establishes a linear relationship between light absorbance (A) and the concentration of the absorbing species (C in mol/L) through the molar extinction coefficient (ϵ) and the optical path length (l, in cm):

$$A = \varepsilon l C$$

UV-Vis spectroscopy is a useful technique to distinguish polyynes with different lengths and terminations, in fact they show recognizable spectra called vibronic spectra [10]. These are characterized by a series of narrow peaks in the UV region, followed by other secondary peaks at longer wavelengths, as shown in Figure 1. 6. Since polyynes are conjugated systems, their absorption spectra are closely correlated to their structure (i.e., the length and the termination groups of the chains) [21]. An increase in the length of the chain corresponds to a decrease in the energy gap and so to a redshift of all the vibronic pattern [22]. The presence of different endgroups affects the absorption spectra. For example, methyl and cyano-endgroups generate a redshift of the peaks with respect to hydrogen-capped polyynes [10].

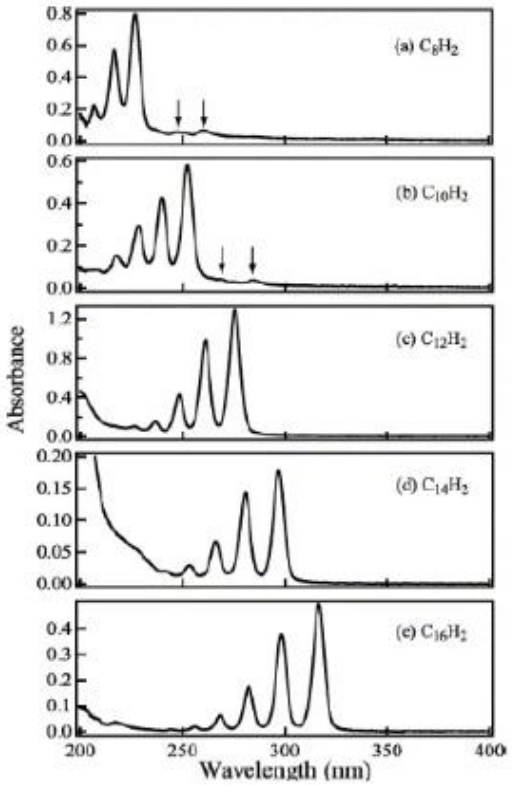

Figure 1. 6 UV-Vis absorption spectra of size-selected H-capped polyynes. The small arrows indicate the presence of impurities [21].

1.5.2. High-Performance Liquid Cromatography

High Performance Liquid Chromatography (HPLC) is a widely used method in chemistry for evaluating product purity and, more broadly, for separating species within a solution [23]. The core of an HPLC system is a porous cylindrical column, into which the sample solution is injected. Within this column, a compact network of porous small particles, such as silica, alumina, and zirconia, functionalized with specific chemical groups forms the stationary phase, interacting both physically and chemically with the sample species. In contrast, the mobile phase, composed of a liquid mixture of solvents, pushes the sample solution through the column, effectively eluting the analytes [23]. The retention behaviour depends on the distinct interactions between the analytes and both the stationary and mobile phases. Physically larger molecules encounter more resistance while going through the densely packed stationary phase. Moreover, the higher the chemical affinity, mainly based on polarity interaction, between the species and the column, the stronger is the retention [24]. Consequently, different molecules within the sample solution are eluted at different times. This time, known as the retention time, is a characteristic parameter in HPLC data. To probe specific properties of the eluted sample, a detection system, that is typically a UV-Vis spectrometer, is integrated at the end of the column [24].

HPLC is mainly used in two possible configurations: normal phase and reverse phase. In normal phase, the stationary phase exhibits polar nature, while the mobile phase is apolar. It is commonly used to analyse polar compounds. Conversely, reverse phase HPLC detects apolar analytes, with an apolar stationary phase and a polar mobile phase [24]. The overall polarity of the mobile phase can be adjusted by varying its composition, significantly impacting the retention time of molecules. When the mobile phase composition remains constant during elution, it is called isocratic mode. If the composition gradually changes, it is called gradient mode [24].

Polyynes characterization via HPLC is typically performed in a reverse-phase configuration, that allows to detect and separate chains with different length and terminations. The apolarity of the stationary phase is obtained by functionalization with hydrophobic alkyl chains, such as C8 or C18, while the polar mobile phase is typically an aqueous mixture with some water-miscible organic solvent, such as Acetonitrile (ACN) or Methanol (MeOH) [10], [25], [26]. Since longer polyynes are more apolar, they have stronger interactions with the column with respect to shorter ones, and in fact they are characterized by longer retention times. Also polyynes of the same length but with different endgroups are eluted at different times, because each endgroup affect the interaction with the stationary phase [22], [27]. In Figure 1. 7Figure 1. 7, a typical chromatogram of polyynes separated by length and termination is shown at different wavelength channels.

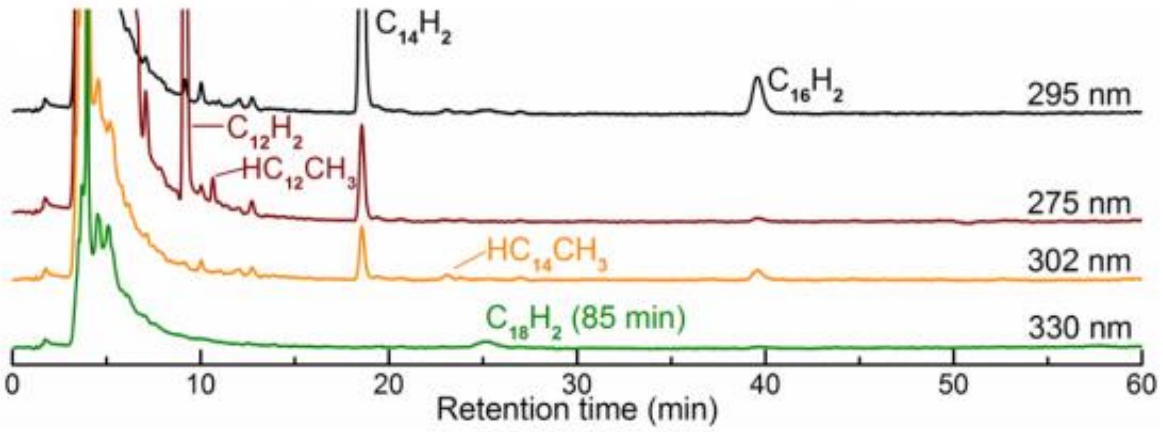

Figure 1. 7 Chromatogramm of polyynes obtained by laser irradiation of toluene. The wavelength of the channels is set on the most intense electronic transitions of polyynes [26].

1.5.3. Raman spectroscopy

Raman spectroscopy, a widely used and powerful technique, exploits the inelastic scattering of monochromatic light, typically a laser, to capture the vibrational transitions of a sample [9]. When an electron in a vibrational state of the electronic ground state absorbs an incident photon, it transitions to the electronic excited state, in the case of resonant Raman spectroscopy, or to a virtual state, as in non-resonant Raman [28]. Subsequently, through a radiative relaxation process, the electron returns to a vibrational state, which may differ from its initial state. So, the photon emitted during relaxation may have different energy from that of the incident one. If the electron relaxes to a vibrational state with higher energy than the initial one, the photon has lower energy, and the process is called Stokes scattering. Conversely, when the electron relaxes to a less energetic state and the emitted photon has higher energy, it is called anti-Stokes scattering [28]. The energy difference from initial and final state, is connected to a specific vibrational state. Since the vibrational structure of a molecule is strongly related to its chemical structure, it represents a fingerprint of the molecule [29]. This fingerprint is visualized as a Raman spectrum, where Raman intensities of the emitted photons are plotted as a function of the Raman shifts (in cm^{-1}).

Since different allotropes show also different vibrational structures, Raman spectroscopy is often used to distinguish and detect the several allotropic forms of carbon, as shown in Figure 1. 8 [2]. CAWs present a recognizable signal related to the collective vibration of all the sp-carbon bonds in the chain (the α or ECC mode), in the 1800-2200 cm^{-1} range. In this spectral region, all the other carbon nanostructures do not present any Raman active modes, thus making the ECC a fingerprint of CAWs [9]. The frequency of the ECC mode is affected by the length and endgroups of the sp-carbon chains. However, if the sample has too low concentration (i.e., lower than 10^{-3} M) of molecules in solution, the Raman signal is too weak, and the molecules are not detectable [9].

This problem is overtaken by exploitation of Surface Enhanced Raman Spectroscopy (SERS), a largely used technique to increase the Raman signal of CAWs [30]. Thanks to the use of metal nanoparticles, SERS exploits excitations of their surface conduction electrons, known as surface plasmons, to enhance the Raman signal up to six orders of magnitude but, because of the interaction between CAWs and metal nanoparticles, it presents shifted and broadened peaks [31].

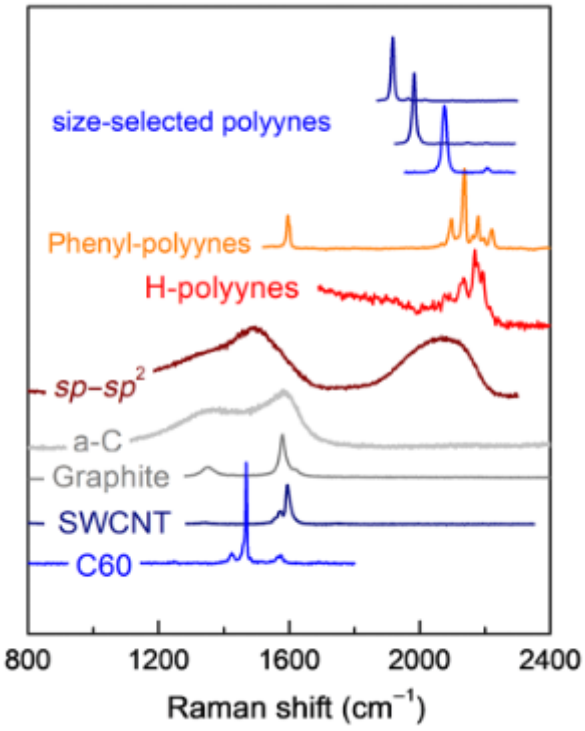

Figure 1. 8 Raman spectra of several carbon allotropes and nanostructures, made of differently hybridized carbon atoms [2].

2 Pulsed Laser Ablation in Liquid

Pulsed Laser Ablation in Liquid (PLAL) is a sophisticated and potent technique that has gained significant attention in the field of material science. This method employs a pulsed laser source to irradiate a target material submerged in a liquid medium. The high energy of the laser pulse ablates the target, leading to the ejection of a plume composed of a diverse mixture of atoms, ions, electrons, and clusters that, by interacting with the liquid environment, rearrange and stabilize forming different nanostructures [32]. The distinguishing feature of PLAL is its unique combination of top-down and bottom-up approaches. The initial process of ablating the target material is a top-down process, where bulk material is broken down into smaller constituents. Following this, the ejected species undergo nucleation and growth in the liquid medium, which is a bottom-up process, leading to the formation of nanostructures [33]. The common PLAL configuration is schematically represented in Figure 2. 1.

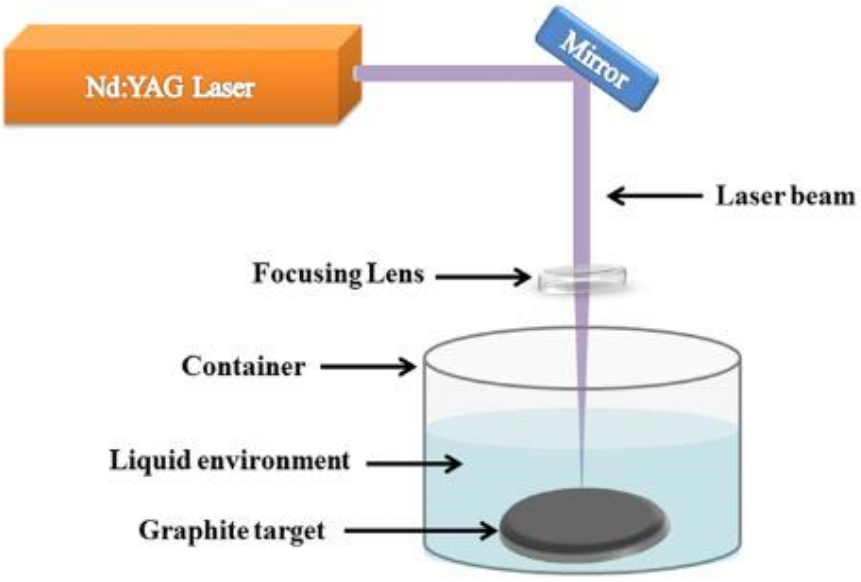

Figure 2. 1 Schematic representation of a common PLAL batch configuration [34].

PLAL was first introduced in 1987 by Patil et al. through the ablation of iron foils in water using a nanosecond laser and in 1993 by Fojtik and Henglein for their work on laser synthesized-colloidal nanoparticles dispersed in a liquid [35], [36]. This technique

is appreciated for its simplicity, scalability, and ability to produce a wide variety of nanostructures without the need for post-synthesis treatments or harmful chemicals [32]. Hence, PLAL adheres to the principles of eco-friendly chemistry. Unlike most chemical synthesis methods that necessitate the use of surfactants, specific solvents, gas environments, and pre- and post-processing steps, PLAL typically operates under normal atmospheric pressure and ambient temperature conditions. It does not require surfactants or harmful substances, and it produces minimal by-products or waste [36].

In the subsequent sections, I will delve deeper into the physical processes involved in PLAL, explore the different configurations of the technique, and discuss its application in the production of polyynes.

2.1. Physical processes involved in PLAL

PLAL is a process where a high intensity pulsed laser is used to ablate a target submerged in a liquid phase. The laser beam, characterized by its high energy density, hits the target surface and creates a plasma resulting in the detachment of extremely hot fragments and atoms from the target surface [37]. As displayed in Figure 2. 2, several phenomena strongly dependent on the laser parameters occur during the process [32] Figure 2. 2 . Hence, a complete understanding of the processes involved in PLAL is still a topic of ongoing research [32].

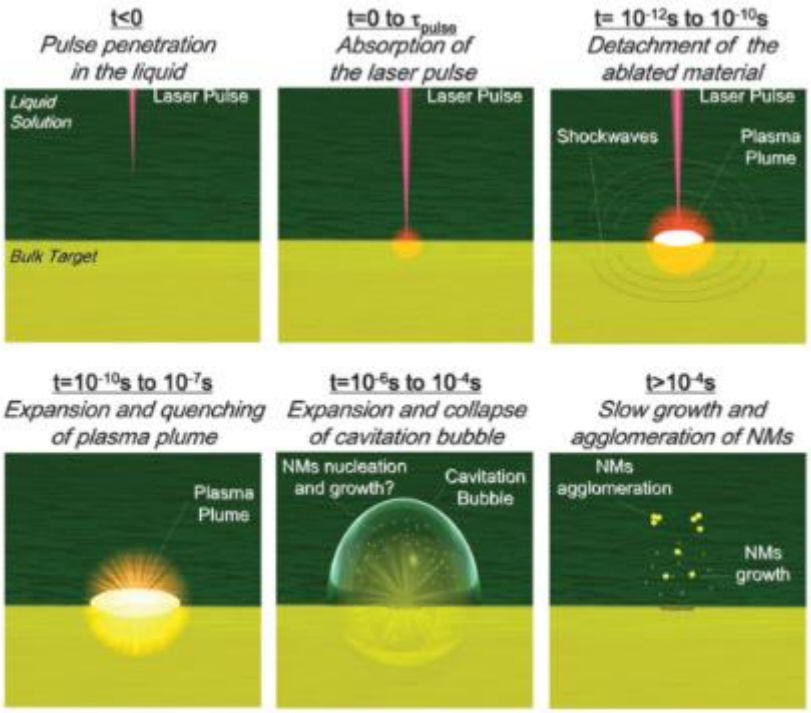

Figure 2. 2 Temporal evolution of the interaction between the laser and a bulk target in PLAL before, during and after the pulse [32].

The first stage of the ablation process involves the laser beam passing through the liquid layer above the target. To ensure the maximum amount of laser energy to reach the target, the choice of the solvent is crucial. The liquid must be transparent to the laser wavelength (minimum amount of photon absorbed) and should not interact with the beam [32]. However, exceptions may arise, for instance, solute compounds might absorb some of the electromagnetic radiation, or synthesized nanomaterials might absorb or scatter part of the laser pulse [32].

It is also important to avoid plasma breakdown of the liquid phase, which can be prevented by using pulses longer than 10^{-12} s (picosecond) and operating under defocused conditions [32], [38]. Additionally, high laser fluences might induce nonlinear absorption effects in the liquid phase, resulting in significant beam attenuation. For instance, in pure water, nonlinear effects such as multi-photon absorption become significant for fluences larger than 70 J/cm2 [39]. Instead, for femtosecond pulses, non-linear optical effects occur at the fluences required for laser ablation, leading to multiphoton absorption by the liquid medium [32]. These nonlinear phenomena can also be affected by the presence of solutes or suspended nanoparticles [38].

When the laser pulse hits the target, both linear and nonlinear absorption effects occur due to the high density of photons [40]. The absorbing material is initially approximated as the volume under the laser-spot area with a thickness equivalent to the skin depth (i.e., the absorbing thickness of the target) [32]. Following absorption, several phenomena occur, such as photoionization due to multi-photon absorption and various thermal processes. Pulses shorter than picoseconds can lead to significant photoionization effects, which are less likely than thermal processes for pulses < 10^{-8} s [32]. Direct photoionization, which happens concurrently with laser-matter interaction, has a timescale comparable with short pulse duration (< ps), resulting in a strong local charge-field and the production of many ionized species and electrons that collide and eject material from the target [32]. In the case of femtosecond pulses, high direct photoionization takes place and numerous electrons are emitted generating highly ionized materials that are split and ejected at high velocities due to charge repulsion, a process known as Coulomb explosion [41]. However, for longer pulses (> picoseconds), thermal processes become more likely, with 10^{-12} s being the characteristic time for electron-lattice thermalization [32]. The energy transfer to the lattice affects a portion of the target larger than the skin depth and phenomena such as thermoionic emission, vaporization, boiling, and melting cause a further material detachment from the target.

Given the multitude of potential fragmentation routes, the ablation mechanism is intricate. As a preliminary approximation, classical thermodynamics suggests three types of thermal processes that result in material separation: vaporization, standard boiling, and explosive boiling [32]. Explosive boiling, also known as phase explosion, is the dominant process for pulses shorter than 10^{-7} s. It involves the superheating of

solid matter to the thermodynamic critical temperature, leading to spinodal decomposition in the irradiated material by homogeneous nucleation [42]. Femtosecond or picosecond pulses sets out-of-equilibrium conditions making a classical thermodynamic description unfeasible.

During the ablation process, the recoil pressure from the ablated material generates two shockwaves propagating within the target and into the liquid, respectively [40]. These shockwaves facilitate material ejection creating discontinuities in density and temperature profiles and heating both the target and the liquid. The ablated material, viewed as an out-of-equilibrium plasma plume, reaches temperatures of 10^3 K and pressures on the order of 10^9 Pa [37]. It is made up by highly ionized species, electrons, as well as molten droplets and solid fragments. The plasma plume is spatially confined to the target surface by the liquid. This results in target ablation not only from the energy transfer from the laser pulse but also from the heating of the plasma plume itself [37]. The energy transfer from the plasma plume continues even after the laser pulse ends. Approximately 10^{-7} to 10^{-8} s after the pulse is generated, the plasma is quenched, and its energy is discharged into the surrounding liquid, causing it to evaporate instantly and form cavitation bubbles, as depicted in Figure 2. 3 Time evolution of a cavitation bubble generated by a Nd:YAG laser ablation of a Ti target in water [43].[32]. These bubbles move at a supersonic speed of 10^3 m/s, expanding and collapsing when the internal pressure falls below the liquid pressure, thus triggering another shockwave. Furthermore, the temperatures and pressures can match those of the plasma plume, leading to the aggregation, phase transitions, and precipitation of the atomic species within the bubble [32].

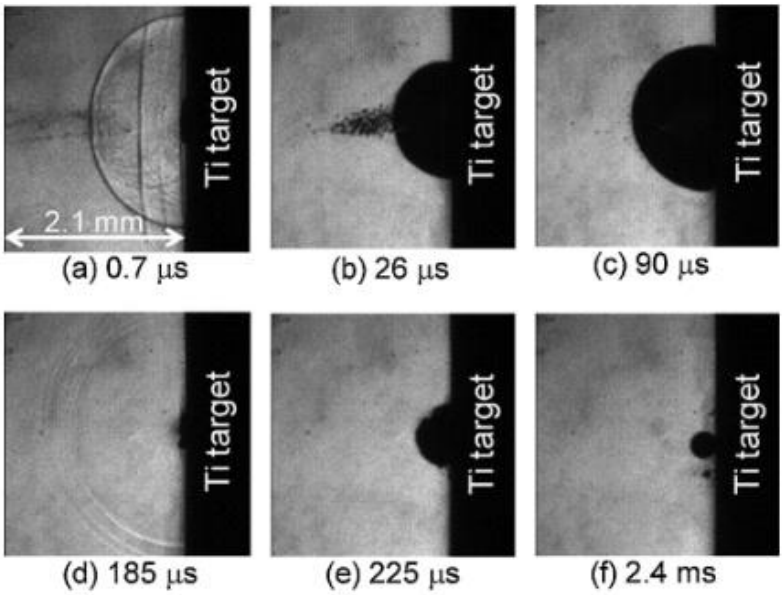

Figure 2. 3 Time evolution of a cavitation bubble generated by a Nd:YAG laser ablation of a Ti target in water [43].

A significant yet unresolved aspect of the physics of laser ablation in liquid relates to the timeframe during which nanostructures are formed. There are varying theories proposing both that nanomaterials move ahead of the cavitation bubbles or that they form inside the bubbles [44], [45]. An alternative theory suggests that, due to the higher thermal conductivity in liquids compared to gases, a temperature gradient is established at the bubble-liquid interface leading to the condensation of nanostructures [46].

2.2. Possible configurations for PLAL

As already discussed, PLAL is a widely used technique due to its ability to produce a variety of nanostructures without the use of ligands. However, the productivity of PLAL is currently limited, and it necessitates the development of strategies to increase production rates, that is fundamental to boost the employment of laser-generated nanomaterials at a large scale [36]. The are different ways to increase the productivity of PLAL. The first approach is the optimization of the laser parameters, increasing the laser power and the repetition rate, and finding the optimum irradiation wavelength for the employed materials [36]. However, when the fluence threshold is exceeded, various limitations that depend on the scanning speed, repetition rate, pulse width, focusing conditions, interaction with the liquid medium, and target geometry appear. Since numerous parameters are implicated, it is difficult to know which of them is the most relevant and this complexity make the system configuration design an important factor for the optimization of the process [36].

There are several configurations that can be used for PLAL, each with its own advantages and disadvantages. The conventional and simplest configuration is the batch production in which the solid target is placed either laying or standing, depending on the direction of the incoming laser, inside a glass beaker or cuvette [36]. This configuration is adequate for producing nanomaterials on a small scale. For larger-scale production, the use of these chambers is no longer feasible since their limited capacity causes the nanomaterials to quickly become concentrated, obstructing the incoming laser beam from reaching the target [36]. The ablated material and persistent bubbles that are created scatter the incoming laser beam, since there is no liquid flow to eliminate them [47]. Another drawback of the batch method is the open top beaker, that can lead to liquid splashing out, potentially damaging the lenses and the mirrors [48]. Therefore, various chamber designs have been proposed to enhance the production rate overcoming these problems [36]. In Figure 2. 4 the main chamber configurations are depicted.

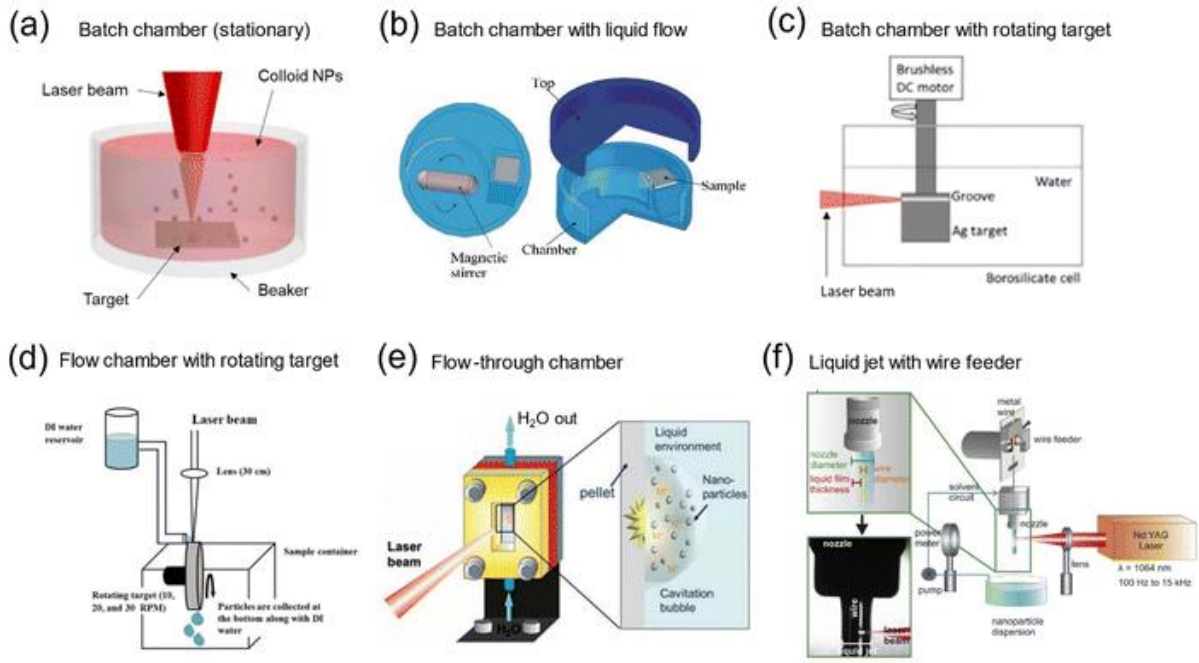

Figure 2. 4 Possible ablation chamber configurations for PLAL: a) stationary batch chamber, b) batch chamber with the liquid flow, c) batch chamber with rotating target, d) flow chamber with a rotating target, e) flow-through chamber, f) liquid jet with wire feeder [36].

The batch chamber with liquid flow (Figure 2. 4b) was first introduced by Barcikowski et al. in 2007 and it is characterized by a magnetic stirrer that generates a liquid flow. This flow inside the chamber aims to cool down the target and displace the generated structures away from the surface of the target, to avoid laser beam shielding [49]. This innovative setup led to a significant increase in the productivity of femtosecond laser ablation, from 0.79 ± 0.36 mg/h in a stationary state to 3.0 ± 0.4 mg/h with liquid flow

[49]. An alternative method involves a rotating cylindrical target in the chamber (Figure 2. 4c), attached to a brushless motor, which creates a liquid flow [50]. This rotation not only moves the generated nanoparticles away from the target but also increases the distance between pulses, reducing the shielding effect of cavitation bubbles. The most efficient PLAL productivity was observed at the lowest rotation speed (300 rpm), with efficiency decreasing as rotation speed increased [50]. This is because higher rotation speeds create unsteady flows and vortices that trap the bubbles produced during PLAL, thereby increasing laser shielding. Another use of the rotating target is depicted in Figure 2. 4d, where it is placed inside a flow chamber, that allows its rotation while the liquid is poured on the ablation spot [51].

The next advancement in chamber design is a flow-through chamber that facilitates PLAL with a continuous supply of fresh liquid and collection of the produced colloid, as shown in Figure 2. 4e [52]. The liquid is pumped through the chamber where ablation occurs, and the created nanomaterials are removed from the chamber, preventing laser shielding. The ideal liquid flow rate is reached when all the nanoparticles are entirely cleared from the ablation area, as confirmed by monitoring productivity with increasing flow rates [36]. A significant benefit of this chamber is its ability to sustain PLAL without reaching colloid concentration saturation, limited only by the target drilling. This allows for extended processing times, even for thin (1 mm) targets. This chamber design can be used in either a continuous line or a closed loop, thus giving rise to two different methods: continuous production and recirculation production, respectively [53]. A detailed analysis and comparison of these two methods will be given in the next section. Different designs of flow chambers have been developed to decrease the thickness of the liquid layer and enable long-term ablation by continuously introducing the target material into the system; an example is depicted in Figure 2. 4f with a jet flow chamber that includes a nozzle and a wire feeder [54]. This innovative method overcomes the primary limitation of the batch chamber for large-scale PLAL productivity, which is the frequent replacement of the liquid as the concentration of the ablated material reaches a saturation point that prevents the laser beam from reaching the target [36]. The other advantage of the jet flow production is the reduction of the liquid layer thickness in the ablation spot [36]. Hence, Sajti C. et al. reported that decreasing the liquid layer thickness from 8 to 2.5 mm improves the PLAL productivity of an α-Al_2O_3 pressed target from 172 to 592 mg h^{-1} [55]. This improvement can be explained since reducing the thickness of the layer above the target reduce the quantity of ablated nanostructures that can interact and absorb the laser beam, leading to a lower reduction of the laser power on the target during all the ablation process [36].

The reduction of the liquid layer can be obtained also in the flow through chamber by a proper design. Both batch and flow through chamber configurations require the substitution or readjustment of the target because of its depletion. Contrarily, a wire target feeder in a liquid jet setup offers the possibility of continuously supplying the

target material while maintaining the benefits of a continuous liquid flow [54]. This setup is expected to be more efficient in the future, as there is no need to stop the ablation process to replace the target and/or the liquid [36]. However, the small size of the wire makes beam alignment more time-consuming and poses a significant challenge compared to the bulk targets in the flow chamber. Furthermore, the stability of the wire feed system and the control of the incident laser fluence present challenges for long-term ablation [36]. Therefore, the described advantages and the ease of handling and alignment make the flow-through chamber design the current standard for PLAL upscaling [36].

2.2.1. Flow through chamber production

As mentioned above, one of the benefits of the PLAL process for nanomaterials production lies in its capability for continuous production. Unlike wet chemical synthesis methods, which typically involve batch production using specific recipes and precise control over reactant quantities and conditions, continuous production in PLAL can be achieved just by employing a flow-cell reactor, with or without liquid recirculation [36].

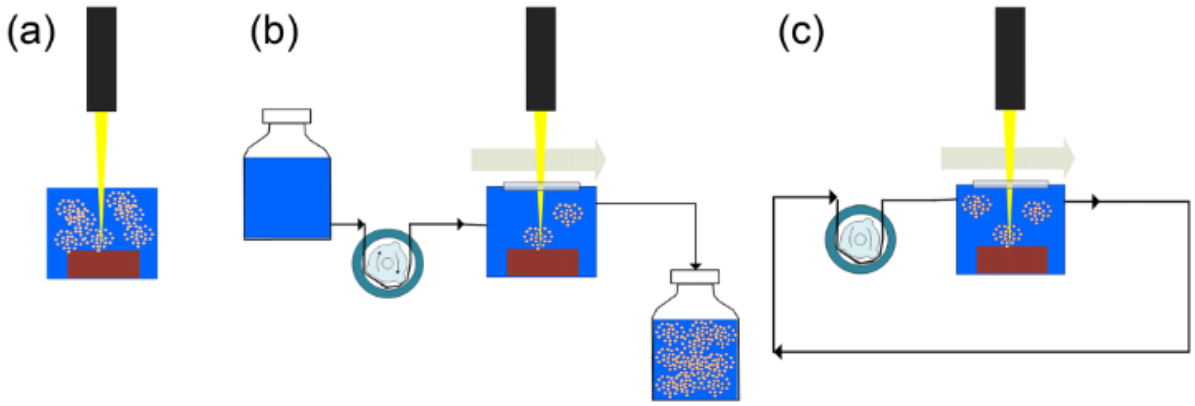

Figure 2. 5 Schematic representation of (a) batch, (b) continuous and (c) recirculation production modes [53].

The two methods of continuous and recirculation production, shown in Figure 2. 5, have been developed to produce silicon NPs (SiNPs) by Freeland B. et al. [53]. The ablation flow-cell, as depicted in Figure 2. 6, was specifically designed to facilitate continuous production across a wide range of volumes, from small volumes (ml) to large volumes (l) of colloids. Its innovative design ensures laminar flow conditions at the ablation site, which help to reduce masking effect of cavitation bubble, plume occlusion, and particle aggregation [53].

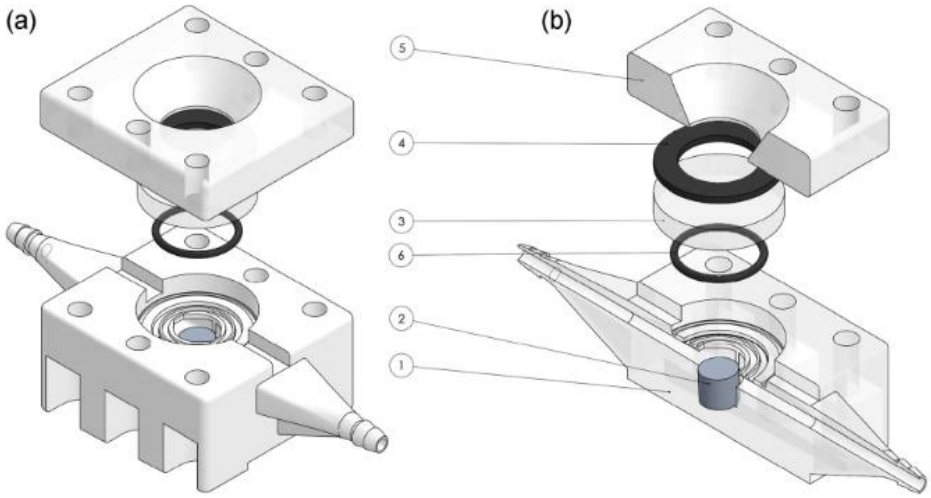

Figure 2. 6 Schematic of the flow-cell design (a) and its cross section (b) including the base (1) target material (2), laser window (3), gasket (4), top-plate (5) and O-ring (6) [53].

The continuous mode of NPs production offers significant advantages with respect to the batch method, as shown in Figure 2. 7. The NPs productivity is increased from 3.5 mg/h achieved in traditional batch mode to 19.1 mg/h of the continuous production [53]. The efficiency of the PLAL process is described by the power-specific productivity (mg/Wh), which is 12.9 mg/Wh for the SiNPs continuous production with respect to 3.63 mg/Wh reported by Kudryashov et al. [56], [53]. The drawback of the continuous flow system is a reduction in SiNPs concentration in the colloid from 73 mg/L (batch process) to 6.8 mg/L. However, 6.8 mg/L is an acceptable concentration for some applications [53]. The efficiency of the system can be attributed to several factors, such as the removal of irradiation shielding effects due to the efficient removal of NPs, microbubbles, and debris from the irradiation site as a result of efficient laminar flow within the flow-cell [54]. Another advantage is the relatively low colloid concentration in the process, that reduces the possibility of a NPs concentration gradients at the ablation site, also reducing the colloid masking effects [57].

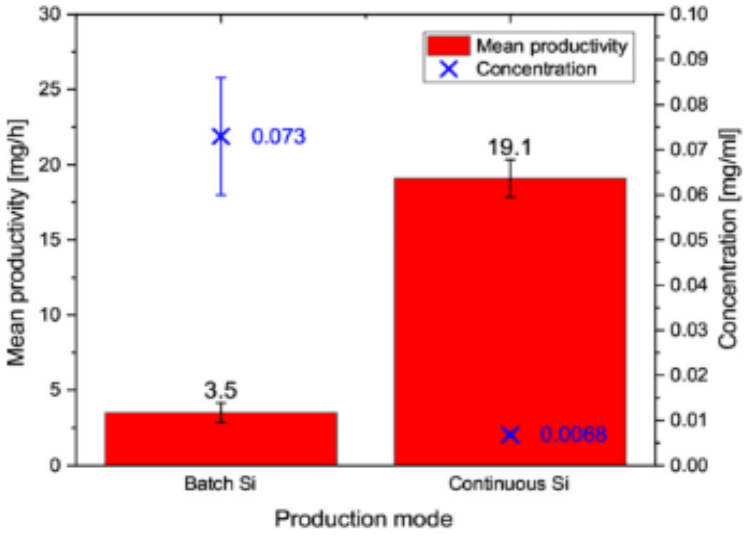

Figure 2. 7 Mean productivity and concentration for SiNPs production in batch and continuous modes, with 50 ml/min flowrate, fluence = 1.83 J/cm^2, Repetition rate = 10 kHz [53].

The recirculation mode can be exploited to produce colloids with high concentrations allowing for 'concentration on-demand' production. The process productivity agrees with the Lambert-Beer law: the NPs concentration increases exponentially but also their shielding effect on laser irradiation is increased, reducing the energy on the target surface [53]. As a result, productivity experiences a logarithmic decline from initial high production rates of 34 to 7 mg/h after 60 min, as shown in Figure 2. 8 [53]. The recirculation tests demonstrate a capacity for the process to produce 83 ml of SiNPs colloid with a selectable concentration up to 91 ± 4 mg/L in 60 minutes, showing a process variation of just 4% [53]. This concentration is higher than the one obtained with the continuous and batch methods, that is 6.8 mg/l at a liquid flow of 50 ml/min for the continuous test explained above, and 30 mg/l for the comparable batch method tested by Kobayashi et al. [58], [53]. Thus, the recirculation mode is suitable for small volume (<100 ml), high concentration NPs production, ideal for the creation of thin films and NPs inks applications [53].

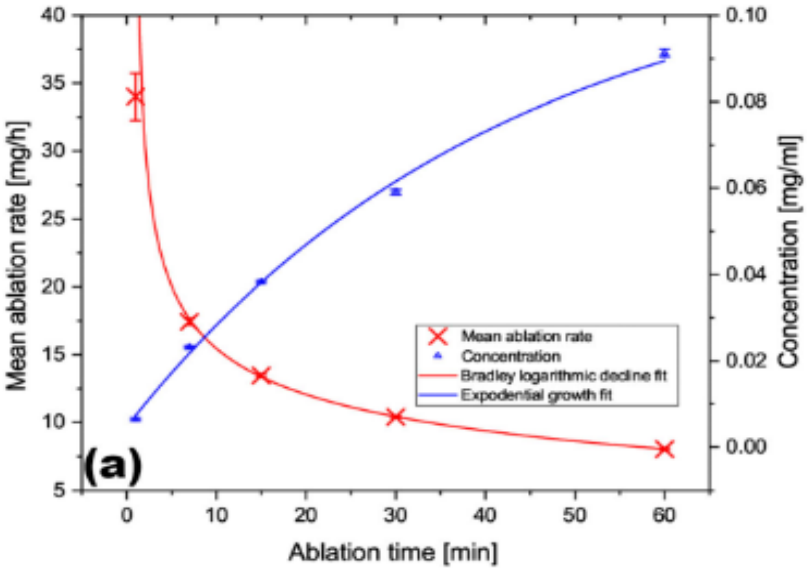

Figure 2. 8 Ablation rate and concentration as a function of the ablation time measured for a 60 min ablation in recirculation configuration [53].

2.3. CAWs synthesis by PLAL

Physical techniques in liquid are very efficient in the production of isolated carbon chains mainly in the form of polyynes, while only rarely has been reported the physical synthesis of cumulenes [59]. Among the physical methods, PLAL is the most used technique. It offers some advantages such as precise control over the ablation parameters and a minimal presence of carbonaceous byproducts in the solution [59]. PLAL is a versatile technique that allows to use non-conducting targets, non-solid targets (e.g., suspensions), or even no target at all by directly ablating the solvent [59]. As a result, this method has been thoroughly studied and improved in the last decades.

2.3.1. Formation mechanisms of hydrogen-capped polyynes

Even though there has been a significant increase in research exploring the properties and synthesis of sp-carbon chains, a complete and fully understood description of the formation of polyynes during PLAL is still missing. Some models have been proposed over the years trying to illustrate this formation mechanisms [60], [61]. The first synthesis of polyynes via laser ablation is reported in the work of Heath et al. in 1987, where they successfully produced polyynes in a gaseous environment [60]. In 1993, Wakisaka et al. demonstrated the simplest growth mechanism of carbon clusters, which is the conversion of two carbon atoms into a C_2 cluster ($2C \rightarrow C_2$), by ablating a graphite target in benzene [61]. Their study did not show any hydrogen-capped polyynes. However, they observed the formation of phenyl rings linked to one or two acetylenic units due to the interaction of carbon clusters with benzene. This observation could be interpreted as the initial stage in the development of stable

phenyl-capped polyynes. In 1996, Gaumet et al. were able to produce C_1, C_2, C_3 and C_4 carbon clusters, as well as phenyl-derived carbon clusters, by ablating a graphite target in benzene [62]. They proposed a model for the formation of aromatic clusters by the addition of clusters to phenyl radicals and for linear clusters by a subsequent addition of C_2 or C. In 2002, Tsuji et al. confirmed this model, specifically for the creation of hydrogen-capped polyynes [63]. According to Tsuji, hydrogen-capped polyynes follow a stepwise growth by the addition of C_1 atoms or larger radical or fragments (from C_2 on), as depicted in Figure 2. 9. Therefore, the two main competing processes in the formation of polyynes are polymerization and termination of the growing chains, which in this case is achieved through the addition of hydrogen atoms, a process known as hydrogenation [59].

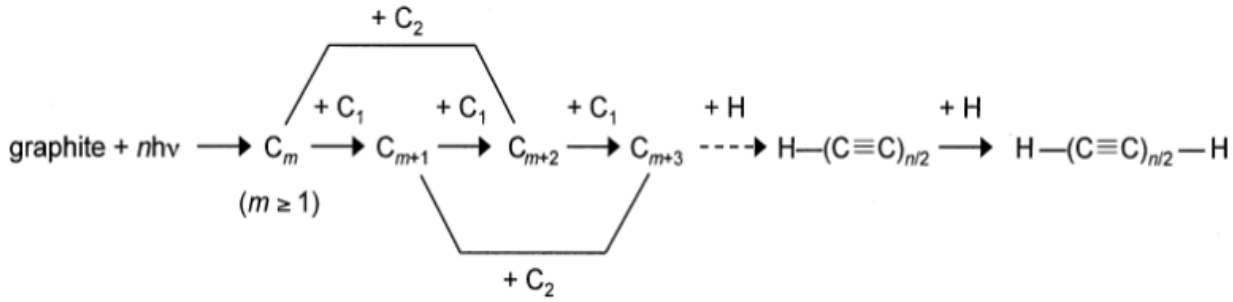

Figure 2. 9 Scheme of the formation of hydrogen capped polyynes during PLAL process [63].

When the target (or the powder) is carbon-based, both the target and the solvent provide carbon atoms or radicals to the polymerization process. Indeed, the intense heat generated by the plasma plume leads to the atomization of multiple atomic layers on the target surface and induces the degradation of the solvent promoting the release of carbon atoms and C_n radicals [59], [10]. Regarding the hydrogenation process, when the target is composed only of carbon (like graphite), the hydrogen atoms or ethynyl radicals C_2H can only be derived from the solvent. The growing chains can be terminated even with atoms different form hydrogens (e.g., CN, CH_3, or more complex radicals) [63]. The solvent used for the ablation is crucial as it establishes the liquid environment for the growth of sp-carbon chains, determining the class of possible terminations, the confinement, and the thermal exchange rate with the plasma plume, as well as the stability of the chains [64]. Thus, in the case of H-capped polyynes their productivity depends on the C/H ratio of the solvent, that for a solvent containing m components is defined as:

$$\frac{C}{H} = \frac{\sum_{m=1}^{\infty} N_A \, n_m N_{C,m}}{\sum_{m=1}^{\infty} N_A \, n_m N_{H,m}}$$

where N_A is the Avogadro number, n_m the number of moles of the m component, $N_{C,m}$ and $N_{H,m}$ the number of carbon and hydrogen atoms contained in the m component, respectively [65]. It's important to note that only hydrogen atoms that are attached to carbon atoms are considered in this calculation. Apart from the liquid environment,

also other ablation parameters strongly affect the yield of polyynes production, such as the pulse duration, wavelength of the laser, pulse energy, ablation time, and target. In the next paragraphs a general description of these parameters is reported.

2.3.2. Laser parameters

Nanosecond (ns) and femtosecond (fs) pulses are the most employed pulse duration in polyynes synthesis via PLAL. Despite the varying dynamics of the overall ablation process, as depicted in Figure 2. 10, there is no concrete evidence suggesting different formation mechanisms of sp-carbon chains when using ns or fs lasers [59]. In fact, the growth mechanism of polyynes suggested by several authors for fs-laser ablation is essentially the same as that for ns-PLAL. Femtosecond lasers allow to reach higher power densities, so intense that the solvent undergoes direct dissociation into atomic, molecular, and parent ions [66]. Thus, in fs-PLAL the laser is focused into the solution and the carbon atoms are provided directly by the solvent degradation [66]. Anyway, for the typical setup with the laser ablating a solid target (the one used in this thesis work) the nanosecond lasers are the most used.

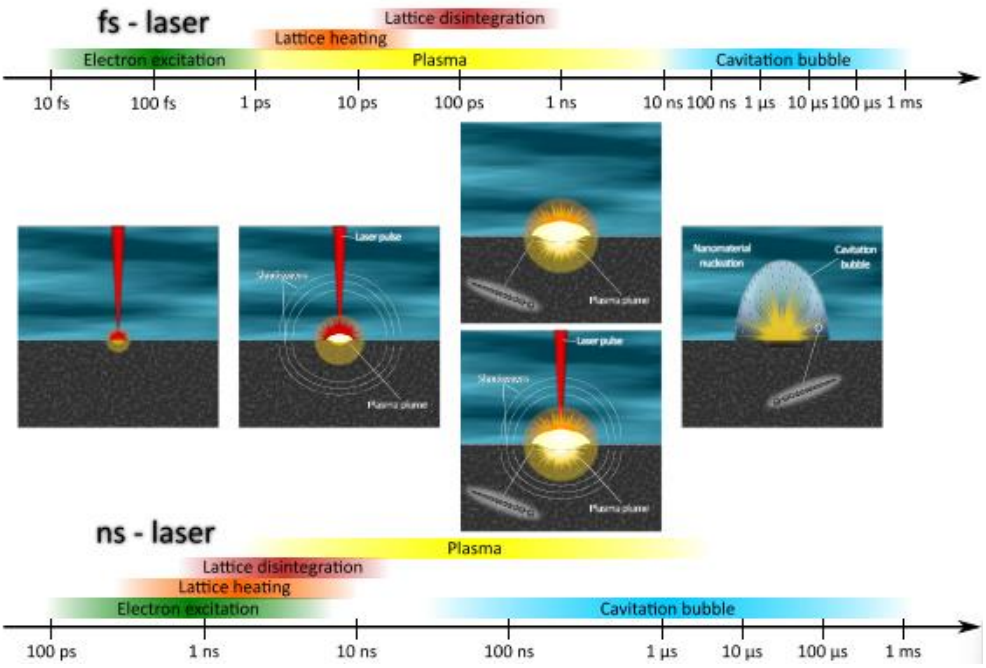

Figure 2. 10 Scheme of the time evolution of the different phases of PLAL by femtoseconds (upper timescale) or nanoseconds (lower timescale) lasers [59].

The commonly used laser wavelengths are 1064 nm, 532 nm, and 355 nm, that correspond to photons in the near-infrared, visible (green), and UV regions, respectively [10], [61]. However, the influence of the wavelength on the yield of polyynes is not entirely understood due to conflicting findings in the literature. Tsuji et al. observed an increase in productivity with shorter wavelengths (266 and 355 nm) when ablating a solution containing suspended graphite particles or fullerenes [63].

Instead, Matsutani et al. found that longer wavelengths resulted in a higher concentration of polyynes when ablating graphite and fullerene pellets in the same solvents used by Tsuji et al. [64]. This trend was also confirmed by Park et al. during the ablation of a graphite target in water [67]. This disagreement is likely due to the different target configurations. Using solid targets, short-wavelength laser beams are more probably absorbed or scattered by impurities or byproducts of the ablation process, which reduces the amount of laser energy that reaches the target [64]. Furthermore, longer polyynes begin to absorb UV lasers and can be broken by the high-energy laser beam [64]. Instead, long-wavelength laser, can penetrate the liquid layer more effectively and is less likely to be scattered by suspended particles or impurities, thus reaching the target with higher energy. As a result, suspended graphite particles or fullerenes, as in the case studied by Tsuji et al., interact with shorter wavelengths lasers increasing the absorption by the carbon particles and enhancing the productivity [59].

The energy delivered by the pulse is another important parameter that can influence the ablation yield. The amount of detached material increases with increasing energy, determining a greater amount of synthesized polyynes [68]. The yield of polyynes is affected by both the pulse energy and the spot size, making fluence one of the most crucial parameters, as depicted in Figure 2. 11. Marabotti et al. recently investigated the connection between these parameters, highlighting the importance of fluence in the synthesis of polyynes [59]. They observed that after a certain threshold, considering a constant spot size, the increase of laser energy, and so fluence, is no more effective. Instead by changing the focusing of the laser beam, different portion of the target can be lit, and hence the amount of material impacted by the laser. Thus, when the fluence of the pulse is kept constant and the spot area is increased, there is a noticeable increase in the volume of ablated material, resulting in a greater yield of polyynes [59]. However, the results can vary for short and long polyynes and using different laser wavelengths, so the correlation between the synthesis yield of polyynes and laser energy is still under investigation.

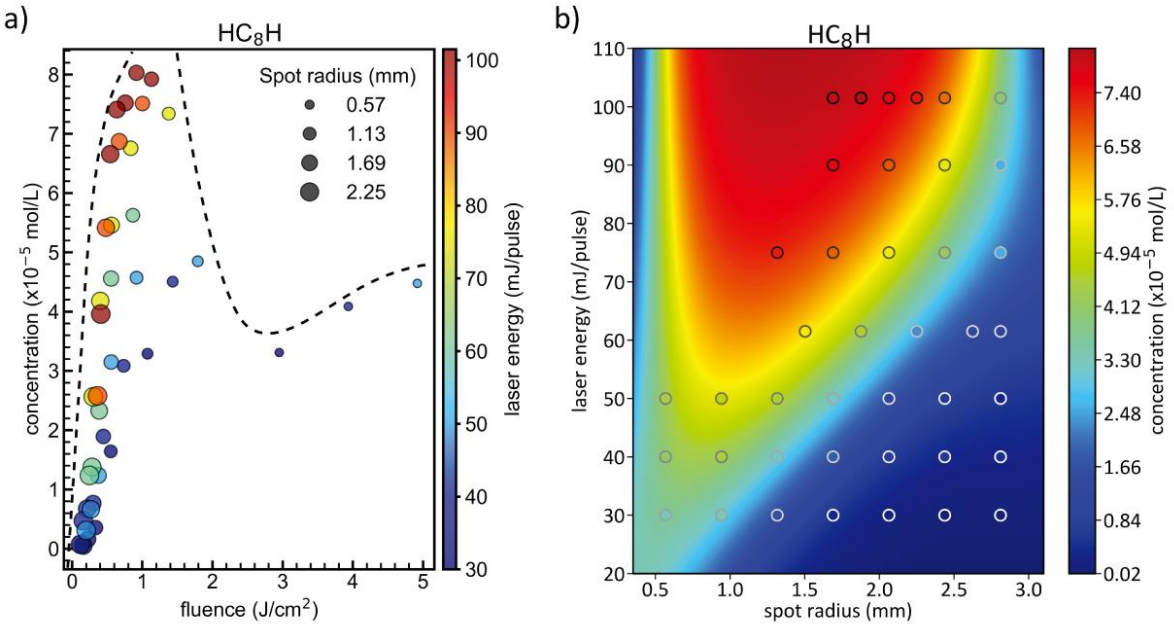

Figure 2. 11 a) Experimental concentration of HC_8H calculated from HPLC analysis of polyyne mixtures obtained by PLAL using different energies and spot sizes (i.e., varying the fluences). The color scale follows laser energy, while the dimension of the circles represents the dimension of the spot radius. b) Same circles as in (a) with a representation of 2D surfaces obtained by a fit of experimental results [59].

In most studies, a repetition rate of 10 Hz is used with nanosecond-pulsed lasers [10], [61]. However, research by Santagata et al. demonstrated that when the repetition rate of the femtosecond laser was increased from 10 Hz to 1 kHz, the production of nanodiamonds was preferred over polyynes [69]. This is likely due to the high pressure created, which stabilizes the nanodiamonds.

Regarding ablation time there are contradictory results found in literature. It is generally agreed that ablation time significantly influences the length distribution of polyynes, although the specifics of this effect are not fully understood. Tabata et al. suggested that longer polyynes are favoured by shorter ablation times, and their formation takes place in the initial stages of ablation [70]. Contrarily, Park et al. found that the concentration of polyynes of any length increases with ablation time [67]. Shin et al. observed a saturation point in polyynes production for ablation times exceeding 30 minutes [71].

2.3.3. Targets and solvents

Targets

Graphite is the most commonly used target material in polyyne synthesis via PLAL. Several forms of bulk graphite, such as rods, disks, or pellets, are utilized according to different studies [64], [10]. Some research, like that of Tsuji et al., has reported the use

of graphite powder suspended in a solution [63]. Matsutani et al. highlight the distinct behavior when ablating a suspended powder versus a bulk target [64]. Graphite powder results in a higher concentration of polyynes, while graphite pellets produce less concentrated but longer polyynes [64]. When ablating a suspended powder, each particle hit by a laser pulse becomes a nucleation site for polyynes, enhancing overall productivity. However, due to the diffusion of ablated material and the movement of graphite particles, the polymerization process is less favored than hydrogenation, leading to shorter chains. Conversely, ablating a pellet produces fewer polyynes but the ones produced are longer [72]. In the case of a graphite pellet, more energy can be focused on its surface. If the production rate of radicals surpasses their diffusion rate, then longer chains are formed [72]. Similarly, graphite cylindrical rods have been observed to produce fewer, but longer, polyynes compared to pellets [72]. This can be attributed to the hardness of the target: the greater hardness of rods results in less dispersion of graphite powder, leading to a lower overall quantity of polyynes, but a higher concentration of longer ones. In fact, Matsutani et al. were able to identify $HC_{30}H$ when ablating the rod, while the longest polyyne produced when using a pellet was $HC_{28}H$ [72]. Other than graphite, a variety of other carbon-based nanostructures have also been successfully utilized. A dispersion of nanodiamonds has been used to produce polyynes up to $HC_{16}H$ [70]. Fullerenes and nanotubes have also been employed in the synthesis process, but only polyynes up to $HC_{12}H$ were observed. In some cases, carbon-based compounds like solid alkanes have been used as targets. Matsutani and his team used a PTCDA (a dye molecule) pellet for ablation and were able to synthesize polyynes up to $HC_{18}H$ in liquid hexane [73].

Solvents

As outlined in section 1.3.1. the liquid phase is a critical factor in the outcome of a PLAL experiment because the properties of the solvent significantly affect the production of polyynes. Several solvents, including deionized water, alcohols, alkanes, acetonitrile, and aromatic solvents, have been used in laser ablations [10][11]. Among them, water is a commonly employed solvent in many works due to its cost-effectiveness, ease of handling, and possibility to obtain a lower concentration of byproducts [67], [74]. However, water does not contain any carbon atoms, which means it does not contribute to the chain growth of polyynes but only to the termination through hydrogen atoms. Hence, only short polyynes are obtained, with the longest polyyne ever detected in water being $HC_{12}H$ [75], [28]. For these reasons, water is considered the least effective solvent in terms of polyynes production [10].

Improved results have been observed with ablations in organic solvents, which have been demonstrated to serve as a secondary source of carbon atoms for the growth of the sp-chains. Laser ablations in pure organic solvents resulted in the creation of polyynes without the need for a target, when using femtosecond pulses. As reported

by Ramadhan et al. [26], polyynes up to 18 atoms were synthesized focusing the femtosecond laser beam on the liquid meniscus. Another important aspect to consider is the rate of hydrogen generation, which plays a crucial role in the termination process. The O-H bond in water molecules, with its higher energy of 4.8 eV, is less likely to break compared to the C-H (4.3 eV), C-C (3.6 eV), and C-O (3.7 eV) bonds found in organic solvents [10]. This implies that the generation of hydrogen in water should be lower, thereby complicating the synthesis process. Thus, as reported by Peggiani et al. in their work [10], the relative amount of hydrogen respect to carbon strongly affects polyynes production, with a higher polyynes concentration for increasing C/H ratios. Figure 2. 12 reported their investigation on the effect of different solvents (i.e., water, methanol, ethanol, isopropanol, and acetonitrile) on polyynes productionFigure 2. 12.

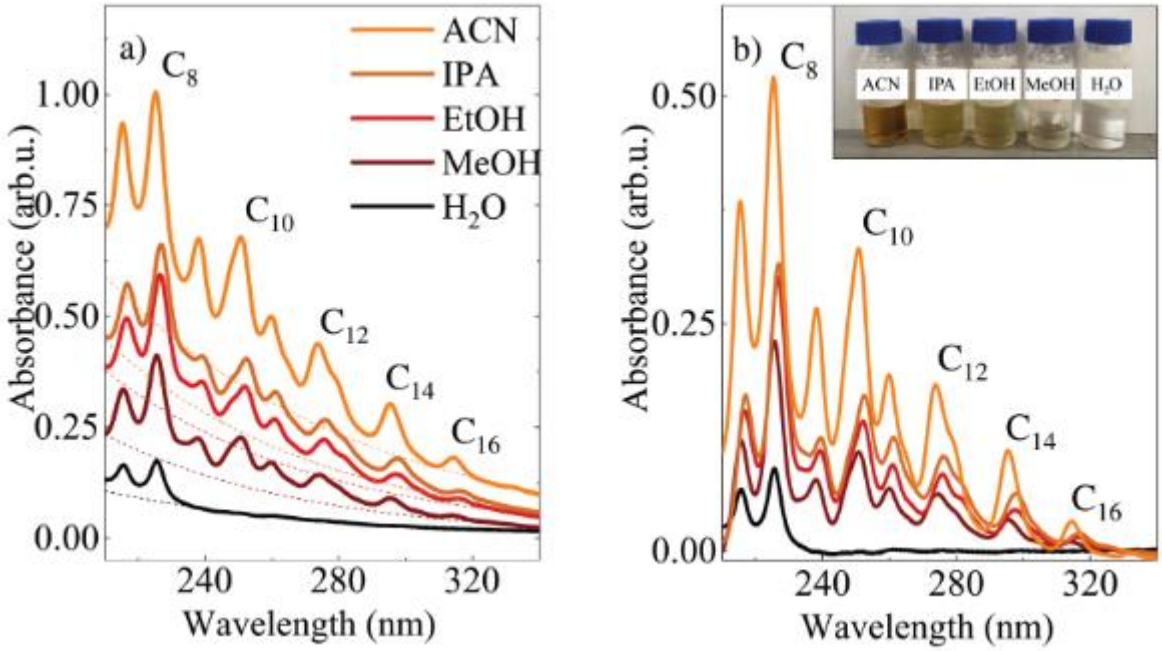

Figure 2. 12 UV-vis spectra of filtered solutions of polyynes in different solvents (i.e., acetonitrile, isopropanol, methanol, ethanol, and water) after laser ablation before (a) and after (b) the background (dotted lines) subtraction. C_8, C_{10}, C_{12}, C_{14}, and C_{16} represent the typical UV-Vis peaks of polyynes composed by 8, 10, 12, 14 and 16 carbon atoms, respectively [10].

Since polyynes are susceptible to oxidation, the quantity of oxygen dissolved in the solvent is also a relevant factor. Oxygen solubility is another important criterion to be considered when selecting a solvent for polyyne synthesis. Peggiani et al. found that acetonitrile results in a greater polyyne concentration than alcohols and water when subjected to a 532 nm laser [10]. This is because acetonitrile has both a lower solubility for oxygen and a higher C/H ratio compared to other solvents. Additionally, acetonitrile is more prone to carbonization than alcohols, which leads to an increased

number of carbon atoms in the plasma, but also results in more hydrocarbon byproducts leading to a higher background in the UV-Vis spectrum depicted in Figure 2. 12. The polarity of the solvent is another important factor that influences the solubility and stability of polyynes. It has been demonstrated that as solvent polarity decreases, the productivity of polyynes increases, as shown in Figure 2. 13 [10]. This result agrees with the work of Matsutani et al. [76], that highlights a strong link between the concentration of polyynes and the polarity of the solvent when ablating PTCDA targets.

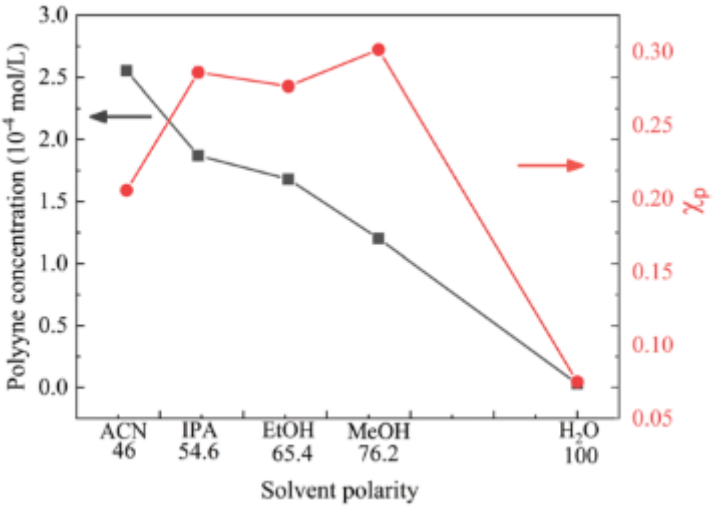

Figure 2. 13 Overall polyyne concentration (mol/L) and index of purity χp plotted as a function of the solvent polarity [10].

Matsutani et al. also highlighted the impact of solvent viscosity on polyyne synthesis. By ablating decalin, a high viscosity solvent, they were able to synthesize polyynes up to the $HC_{30}H$ [76]. High viscosities impede the diffusion of ablated species, potentially leading to a higher concentration of C_2 radicals in the plasma plume and an increase in polymerization. Furthermore, the high C/H ratio of decalin facilitates polymerization due to a lower concentration of hydrogen [76].

Another factor related to the nature of the solvent is the possibility of obtaining terminations different than hydrogen. Polyynes terminated with deuterium were produced in deuterated water [77]. Cyano-polyynes (HC_nCN) have been identified when acetonitrile was used as the solvent [11]. Methyl-polyynes (HC_nCH_3) were synthesized ablating in hexane, alcohols, and toluene [78], [26].

3 Materials and Experimental Methods

This chapter is structured into two parts. The first part provides a detailed description of the materials (i.e., the targets and the solvents) employed in the experiments conducted for this thesis. The second part focuses on the experimental procedures employed for the synthesis and characterization of polyynes. Thus, a description of the PLAL setup and system configuration is given and the most relevant characterization methods used in this work (i.e., HPLC and UV-Vis) are described.

3.1. Materials

3.1.1. Targets

The correct choice of the target is important since it is the primary source of ablated materials in the PLAL process. In this work, a bulk graphite target was chosen because, as described in literature, it is a reliable and non-toxic source of carbon. All the targets used are 99.99% pure (Testbourne Ltd). Most of the experiments were conducted with a target of 10 mm in diameter and 3 mm in thickness, that fit the inner dimensions of the flow-cell used for the PLAL experiments in flow regime. A few additional experiments were performed with a bigger target, measuring 50.8 mm in diameter and 5 mm in thickness, suitable for the glass beaker used for the PLAL experiments in static conditions. A picture of both the targets is given in Figure 3. 1.

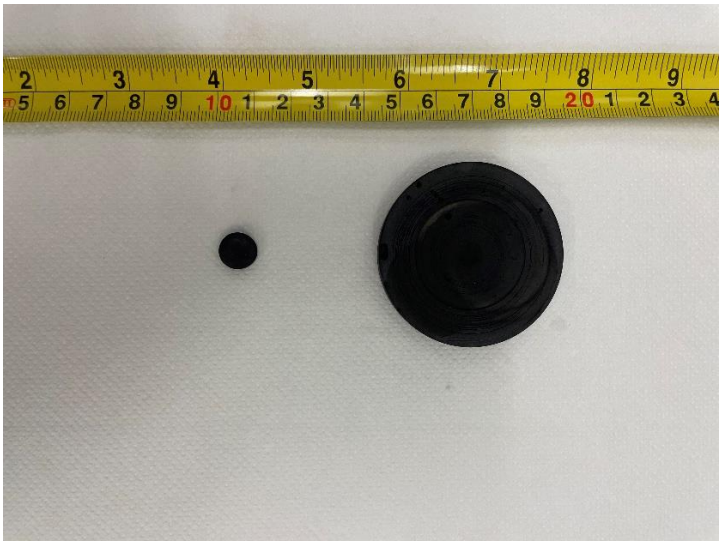

Figure 3. 1 Picture of the two graphite targets used for ablations.

3.1.2. Solvents

Two different organic solvents were employed as liquid media for the ablation: methanol (MeOH) and acetonitrile (ACN), which chemical formulas are represented in Figure 3. 2. Being organic, these solvents can provide secondary carbon atoms during the PLAL process, increasing the production and stability of polyynes, and have already been widely used in literature [10]. The solvents used in this work are characterized by an HPLC-grade purity (≥ 99.9% provided by Sigma-Aldrich), ensuring a high compatibility with the HPLC system and preventing interactions of polyynes with impurities during the ablation process. Since HPLC is employed as a characterization method, the choice of the organic solvents is constrained by their compatibility with the HPLC columns and mobile phases. The main properties of these solvents are described in Table 3. 1.

Table 3. 1 Main properties of the solvents used for ablation experiments.

Solvent	**Density [g/cm3]**	**Viscosity [◦C]**	**Refractive index**	**Dielectric constant**	**Ostwald coefficient**	**UV cut-off [nm]**	**C/H ratio**
MeOH	0.792	0.60	1.326	32.6	0.2476	205	0.33
ACN	0.782	0.38	1.342	37.5	0.00083	190	0.66

Figure 3. 2 Chemical formula of methanol (on the left) and acetonitrile (on the right)

Among the two solvents used in this work, ACN leads to a higher concentration of polyynes but presents a lower 'index of purity', mainly due to the higher C/H ratio and lower polarity, as reported in the work of Peggiani et al. [10]. Instead, MeOH used in their work showed the lowest concentration of polyynes but the highest 'index of purity' between the other organic solvents employed.

In this work, the solvent volume used for the ablations was fixed at 100ml, that is the lowest volume suitable to guarantee a constant flow with the system configuration that I designed. The choice of using the lowest volume is dictated by the need of optimizing the consumption of the solvents and to have a higher concentration of

polyynes. This setup and the several choices regarding the solvents will be better discussed in the next chapter.

3.2. Pulsed Laser Ablation in Liquid

The experimental setup of Pulsed Laser Ablation in Liquid (PLAL) used in this thesis work is shown in Figure 3. 3. The laser is a Quantel Q-switched Nd:YAG ns-pulsed laser with a repetition rate of 10 Hz and a pulse duration of 6 ns. Its fundamental wavelength is 1064 nm, but also different harmonics can be used, such as 532 nm and 355 nm, by using second and third harmonic generator modules, respectively. The maximum nominal energy per pulse is 850 mJ for the fundamental harmonic, 430 mJ for the 532 nm, and 230 mJ for the 355 nm harmonic. Due to the long-time ablations performed in all the PLAL experiments during this work, it was preferred a laser wavelength (1064 nm) able to minimize the interaction with the particles in solution (i.e., reducing the masking effect). This choice is more important with ACN, that shows a low index of purity, as better explained in section 2.3.2. With this setup, it is possible to tune the pulse energy thanks to a beam attenuator with the aid of a power meter, allowing to perform most of the experiments with different energies. During the ablation, the laser beam is emitted horizontally from the laser head, then is deviated by a 45° mirror (Lambda Research Optics, Inc.) to go down toward the focusing lens and then to the target. Two focusing lenses were used in this work, with 15 and 20 cm focal length. In both the focusing conditions, the spot size of the laser beam on the target surface can be controlled by changing the distance between the lens and the target. This is possible since the beaker, or the cell, containing the target is placed on a stage composed by three translators able to move in the three dimensions and controlled by a custom Python code. Through the movement of the vertical translator (z-axis), the distance between the focusing lens and the target can be modified, resulting in a reduction of spot size when this distance is increased, until it reaches the same value of the focal length, where ideally the spot is a dot. The lens-target distance was automatically set by the custom Python code, that calculates it depending on the given input parameters, such as desired spot size, refractive index of the solvent, solvent volume and height in the ablation site, and geometrical features. For some experiments, the ablation was done without the focal lens and the target was hit by a non-focused beam with a diameter of 9 mm. The stage also allows to move the target during the ablation to have a more homogeneous target consume, keeping the ablation chamber in a uniform spiral motion.

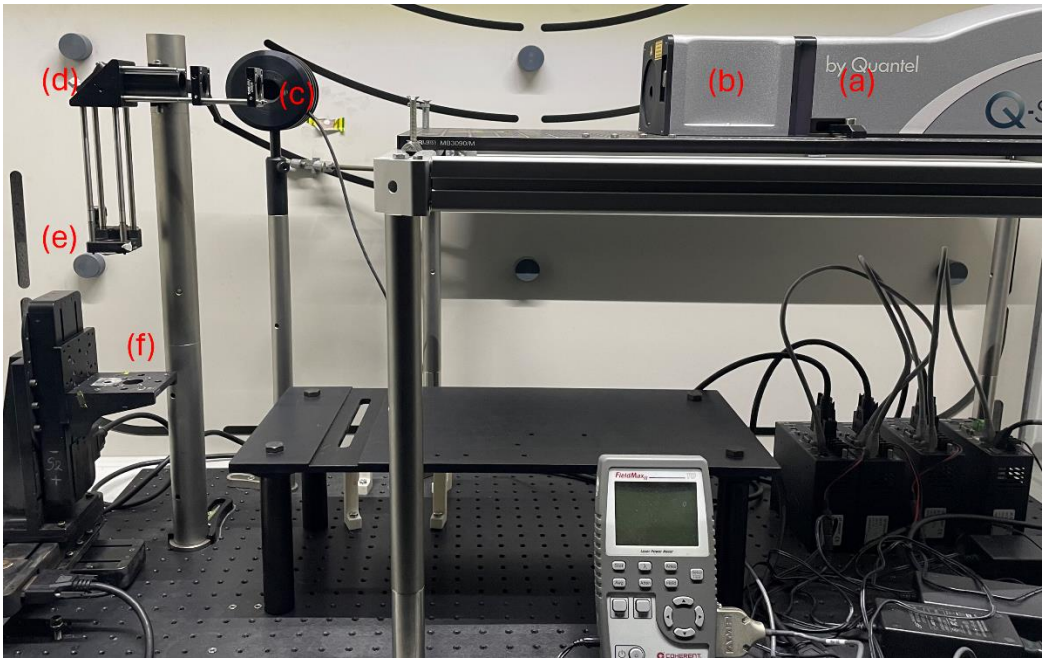

Figure 3. 3 PLAL experimental setup: (a) the laser head, (b) the beam attenuator, (c) the power meter, (d) the 45° mirror, (e) the focusing lens, and (f) the stage.

In this work, as told in 3.1.1., the most employed PLAL configuration was the one in flow conditions (see Figure 3. 4b.), that includes a flow through chamber, where the target is placed, and a pump system, allowing for a recirculation mode production. For comparison, other experiments were conducted in static conditions (Figure 3. 4a) where the ablation site is composed by a big glass beaker placed on the stage, that contains both the solvent (100 ml) and the big graphite target on the bottom. In both cases the stage moves the ablation chamber in spiral motion, unless when the flow cell is used in unfocused condition because the diameter of the laser beam is almost equal to the target diameter, so there is a geometrical limitation. The flow cell used for the recirculation production is a home-made Teflon cell (100x30x30 mm) designed to guarantee laminar flow conditions and chemical compatibility with the solvents employed in PLAL. The pump system includes a magnetic dosing pump GMXa (Prominent), that is a membrane pump with high compatibility with organic solvents able to generate a reliable flow, and three tubes, that connect the different parts of the system, making the recirculation of solution possible. The tubes employed are made up of Teflon, and they show high chemical compatibility with the solvents and a good grade of transparency, in order to monitor the liquid flow.

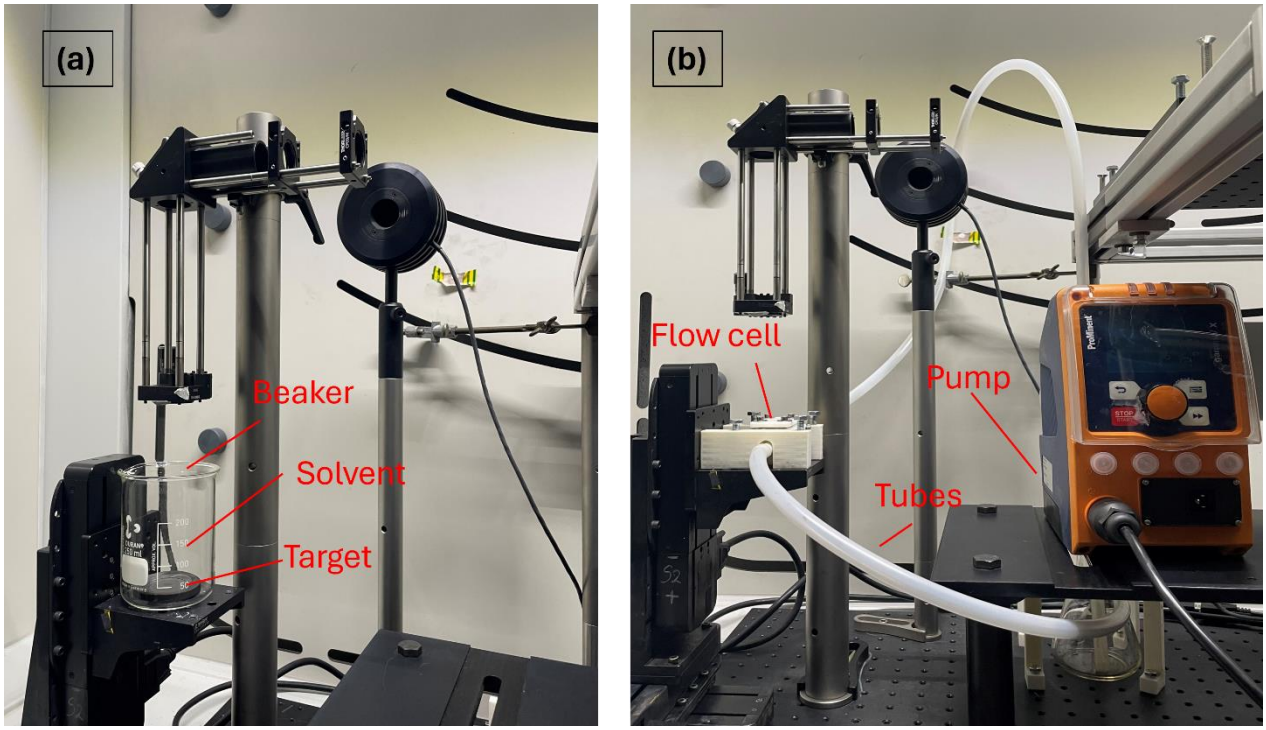

Figure 3. 4 PLAL setup in the two configurations: a) static condition and b) flow condition

3.3. Characterization methods

Polyynes solutions obtained in this work were characterised with UV-Vis absorption spectroscopy and HPLC. These systems are described in the following sections.

3.3.1. UV-Vis absorption spectroscopy

UV-Vis absorption spectroscopy is one of the easiest and fastest characterization techniques for polyynes, thanks to their strong optical absorption that results in a characteristic absorption spectrum. The instrument used for this work is the Shimadzu UV-1800 spectrophotometer, that allows for measurement of the samples in a broad spectral range, from 190 to 1100 nm. It is equipped with two lamps: a deuterium lamp for the UV region (from about 190 to 400 nm) and a tungsten lamp for the visible and near-IR ranges (until 1100 nm). In this thesis work, most of the measurement were done in a spectral range from 190 to 600 nm, since the signals related to polyynes are in the UV region. Few spectra have been done in the whole range to observe the optical absorbance of the sample at 1064 nm, that is the laser wavelength used for all the ablations.

To avoid saturation of the detector, each ablated solution has been analysed after diluting with the respective pure solvent in a ratio 1:20, thus mixing 40 µl of polyynes solution with 760 µl of pure solvent. The sample was put in a quartz cuvette with an optical path of 10mm, because of quartz transparency in the whole measurable region.

The absorption of the samples is determined by subtracting the absorption of a reference solvent or solution. This is achieved by placing the reference in an optical path designated as "reference" and conducting simultaneous measurements with the sample. Every analysis of polyynes solution were done with a reference of pure solvent to remove the background of the solvent itself. Each solvent presents a characteristic cut-off wavelength, that is the wavelength below which its absorption is too intense to give a reliable signal. For the solvents selected in this work, as shown in Table 3. 1, the cut-off is quite low, allowing to detect also chain containing 6 sp-carbon atoms in the case of ACN, and 8 sp-carbon atoms for MeOH. With UV-Vis spectroscopy it is also possible to estimate the polyynes concentration by applying the Lambert-Beer law.

3.3.2. High-Performance Liquid Chromatography

High-Performance Liquid Chromatography (HPLC) is a widely used characterization technique that allows for separating, identifying, and collecting all the polyynes produced during the ablations by their lengths and terminations. In this thesis work, to calculate more precisely the concentration of the different polyynes in the analyzed sample with respect to UV-Vis spectroscopy, a reverse-phase liquid chromatography (RP-HPLC) was used, because polyynes better interact with non-polar stationary phase. The employed instrument was a Shimadzu Prominence UFLC (in Figure 3. 5) equipped with a SIL-20A autosampler, which automatically withdraws and injects the sample in volumes ranging from 1 to 500μL; a LC-20AT high-performance pump capable of exerting a maximum pressure of 400bar; a CTO-20A column oven to store the columns at a constant temperature during the analysis; SPD-M20 photodiode array UV-Vis spectrophotometer serving as a diode-array detector (DAD); and a FRC-10A fraction collector for collecting polyynes of different sizes and terminations. The UV-Vis spectrometer has two lamps (deuterium and tungsten lamp), that allow to measure in a range from 190 to 800 nm. The core of the instrument is the column that contains the stationary phase. The one employed to perform the analysis is the Phenomenex Luna C18 (150 mm x 4.6 mm), that is an analytical column made up by packed silica particle of 5 μm size functionalized with alkyl ligand chains of 18 carbon atoms, which are responsible of the apolar character of the stationary phase.

Figure 3. 5 HPLC apparatus employed in this work: the autosampler (a); oven and columns (b); the fraction collector (c); the pump system (d); the photodiode array spectrometer (e); the controller (f); solvent tray (g)

Before the analysis, each sample was filtered using a PTFE syringe filter (Phenex, 0.45 μm pore size) to remove bigger impurities contained in the ablated solution that might obstruct or damage the column. All the ablations were examined using a gradient method on the Luna C18 column. This method employed a mobile phase of ACN and water, starting with an initial ACN percentage of 65%, which was gradually increased to 95% for 20 minutes, and then kept constant until the end of the analysis at 45 minutes. The gradient method was preferred instead of the isocratic one, because it guarantees a higher resolution and separation of shorter chains. The flow rate of the mobile phase was set to 0.8 mL/min, and the sample injected volume was 15 μL.

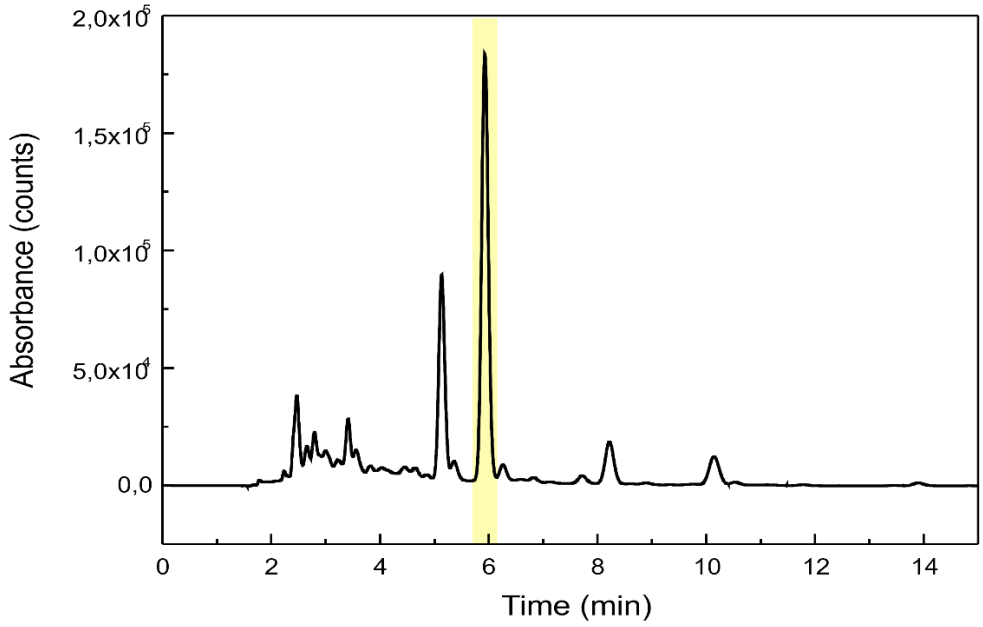

Figure 3. 6 Chromatogram at the fixed wavelength of 226 nm. The highest peak represents the MIT of HC_8H.

The result of the HPLC analysis is the so-called chromatogram, a plot of the absorption versus elution time at a certain wavelength. Thus, by setting a specific wavelength, the chromatogram displays a series of peaks corresponding to the species that absorb at that wavelength, as depicted in Figure 3. 6. Since absorption is linked to the concentration of the species (i.e., Lambert-Beer law), the concentration of each species can be determined by measuring the area of each peak. Each polyyne has its own wavelength where the Most Intense Transition (MIT) takes place. The main MIT wavelengths of H-capped polyynes are reported in

	C_6	C_8	C_{10}	C_{12}	C_{14}	C_{16}	C_{18}	C_{20}
MIT wavelength [nm]	198	226	251	273	295	315	332	348

Table 3. 2. Therefore, a channel for each characteristic wavelength was established in the HPLC program, and the chromatographic area of each peak associated with polyynes was measured at its own MIT wavelength. Thus, thanks to a calibration model, it is possible to correlate the concentration of each sp-carbon chain to its chromatographic area.

	C_6	C_8	C_{10}	C_{12}	C_{14}	C_{16}	C_{18}	C_{20}
MIT wavelength [nm]	198	226	251	273	295	315	332	348

Table 3. 2 MIT of H-capped polyynes ranging from 6 to 20 sp-carbon atoms.

4 Experimental Results

In this chapter, I will present the results obtained from the experimental work. To the best of my knowledge, no previous works reported an investigation on polyynes production by PLAL in flow conditions. The recirculation system has only been explored in literature for PLAL production of nanoparticles (NPs), showing interesting results for the scale-up of this technique, as better discussed in section 2.2.1. This optimization of NPs production may suggest that also an optimization of polyynes production through a recirculation system is possible. To reach this challenging result, I designed a recirculation system able to guarantee a reliable flow, an appropriate ablation site, and safe working conditions. In the first part of this chapter, I will discuss all the choices done to find the optimal design, delving into the different cell configurations tried in the experiments, the compatibility of the apparatus with the solvents, and the glass interaction with the laser beam. In the second part, the focus will be on the optimization of polyynes production describing how the solvents and the configurations affect the production and once selected the optimal conditions, investigating the effect of different laser parameters- such as pulse energy, spot radius, and fluence- on polyynes concentration in the final solution. In the last part I will present the best results obtained through the recirculation system comparing them with the ones obtained in the static configuration, explaining the possible reasons and hypotheses on the differences experimentally found.

4.1. Recirculation system design

As shown in section 3.2., the setup of the recirculation system is mainly composed by a flow cell, a membrane pump, three connecting tubes, and a glass beaker where the solution is collected. The pump is the motor of the system, since it withdraws the liquid from the beaker placed below and moves it into the tube connected to the outlet on top of the pump. The liquid is pushed by the pump until the curve of the tube, where the liquid starts falling towards the cell, passing through it and then going back to the beaker through another tube (see Figure 4. 1). Thus, the liquid flow falling to the cell is mainly due to gravitation, and it is not only governed by

the pump but also depends on the height of the tube. To ensure fluent working conditions, this system requires a well-designed configuration where the tube extends upward to a specific height before descending to the cell (see Figure 4. 1). This design allows for the creation of a tall liquid column above the pump outlet, effectively preventing air bubbles from entering. The flow generated is not continuous, because of the working principle of the pump, based on a membrane that moves back and forth creating two strokes: the downward stroke to draw the liquid, and the upward stroke to move the liquid out from the outlet of the pump. The strokes frequency and duration can be regulated by a manual controller. Since these parameters affect the flow inside the cell, I set them to improve the continuity of the flow. In most of the experiments the pump was set to 130 strokes per minute and 30% of stroke duration, since increasing the frequency and reducing the duration leads to a more homogeneous flow. These parameters, together with the cell design, also determine the liquid volume inside the cell, thus the height of the liquid layer above the target, that is fundamental for the PLAL process. However, since the tubes are not completely fulfilled and the system is not on pressure, the flow velocity, the flow rate, and the liquid volume in the cell are not narrowly controlled.

Figure 4. 1 Picture of the PLAL setup in flow condition with highlighted the height of the tube on top of the pump that contains the liquid column.

4.1.1. Materials compatibility with the solvents

The various components of the recirculation apparatus must be compatible with the solvents employed in the experiments, namely methanol and acetonitrile. The membrane pump is certified to be compatible with these organic solvents. Additionally, the cell was designed using Teflon (PTFE) to ensure such chemical resistance. However, the three possible tubes did not guarantee this compatibility, so I analysed them to test their interaction and eventual degradation with the solvents. Specifically, I refer to the three tubes as: PTFE tube, semi-rigid tube, and silicon tube. A small portion of each tube have been immersed in a vial containing 10 ml of the two solvents. Subsequently, at intervals of 30, 150, and 210 minutes, the tube was extracted performing UV-Vis analysis on the solutions. The obtained UV-Vis spectrum was then compared with that of the pure solvent. If noticeable differences exist between the two spectra, it indicates that the tube is dissolving and altering the UV-Vis signal. The results of the analyses conducted using this procedure are summarized in Table 4. 1 and shown in Figure 4. 2.

	PTFE	Semi-rigid tube	Silicon tube
MeOH	Not dissolved	Dissolved	Dissolved
ACN	Not dissolved	Dissolved	Dissolved

Table 4. 1 Results of the compatibility test performed on the three tubes immersed in methanol (MeOH) and acetonitrile (ACN).

Notably, the PTFE tube remains undissolved even after 210 minutes. In contrast, the other two tubes exhibit a distinct peak in the spectrum only after 30 minutes, which is absent in the pure solvent spectrum. This peak arises due to the dissolution of the tubes. Therefore, I decided to use the PTFE tubes as connecting part of the recirculation system for this work.

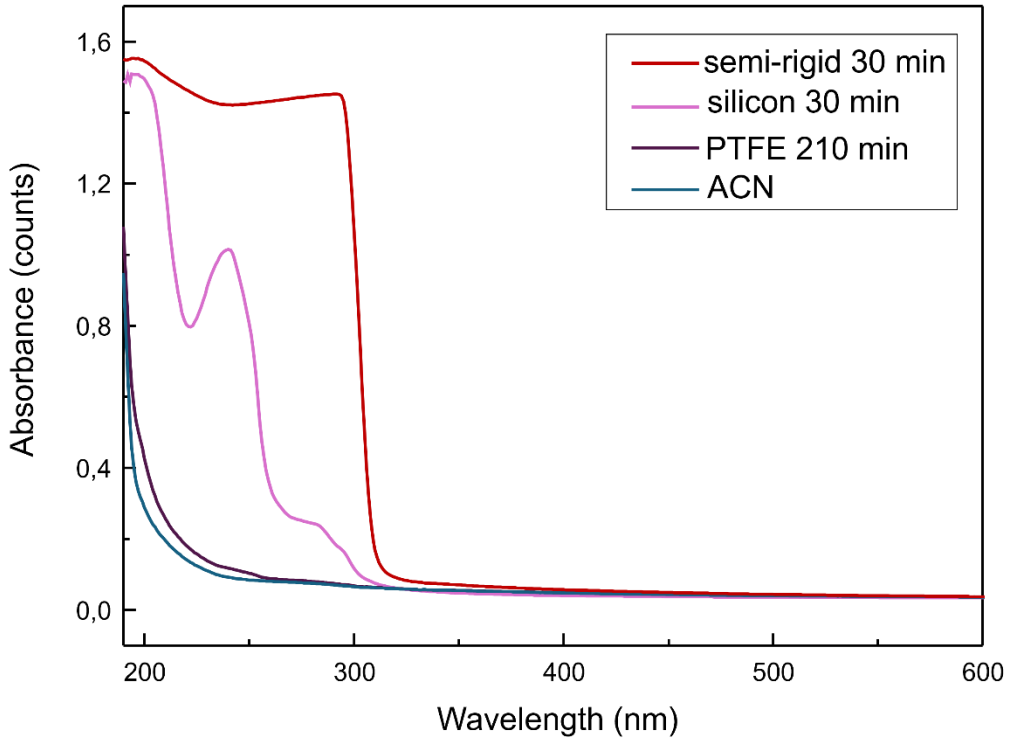

Figure 4. 2 UV-Vis spectra of the solutions containing the silicon tube, the semi-rigid tube, and the PTFE tube, with respect to the spectrum of the pure ACN.

4.1.2. Glass-laser interactions

In all the configurations described above, the laser beam must pass through a glass window to reach the target placed inside the cell during ablation. The wavelength used in all the experiments is 1064 nm, and the glass is transparent at this wavelength. The glass absorption was tested using UV-Vis absorption analysis covering the entire range of wavelengths from 190 to 1100 nm. The obtained spectrum, shown in Figure 4. 3, does not exhibit any absorption peak at 1064 nm. However, in the case of intense laser pulses, the glass may absorb due to nonlinear phenomena increasing the fraction of absorbed energy even at wavelengths where absorption is negligible for lower intensities. Indeed, several materials are transparent at low or moderate optical intensities but become strongly absorbing once the threshold for laser-induced breakdown is exceeded [79]. The involved process may start with multiphoton absorption, which generates some free carriers, and these can subsequently provide strong linear absorption for further radiation [79]. Furthermore, the physical mechanisms of laser damage may depend on the pulse duration. For nanosecond pulses, non-deterministic damage is often

observed, where the probability of damage increases smoothly around the threshold [79]. The laser threshold depends on several factors, such as energy, spot size, and pulse duration, making it challenging to directly compare with existing literature. Consequently, I investigated the glass-laser interaction at various fluences to determine the damage threshold of the glass used in our setup. This information is crucial for ablation procedures, as it provides an upper limit on fluence beyond which the system cannot be safely used. The fluences were calculated on the glass surface by dividing the pulse energy by the spot area. When subjected to a laser beam with an energy of 200 mJ/pulse and a spot radius of 1.7 mm, corresponding to a fluence of 2.5 J/cm², for 30 minutes the glass exhibited no apparent damage. Instead, repeating the experiment with a reduced spot radius of 1.5 mm, resulting in a fluence of 2.8 J/cm², the glass revealed clear signs of damage after only 3 minutes, as depicted in Figure 4. 4. Therefore, the fluence limit in this case lies between 2.5 and 2.8 J/cm², that is the approximate critical value for the ablations conducted in this configuration.

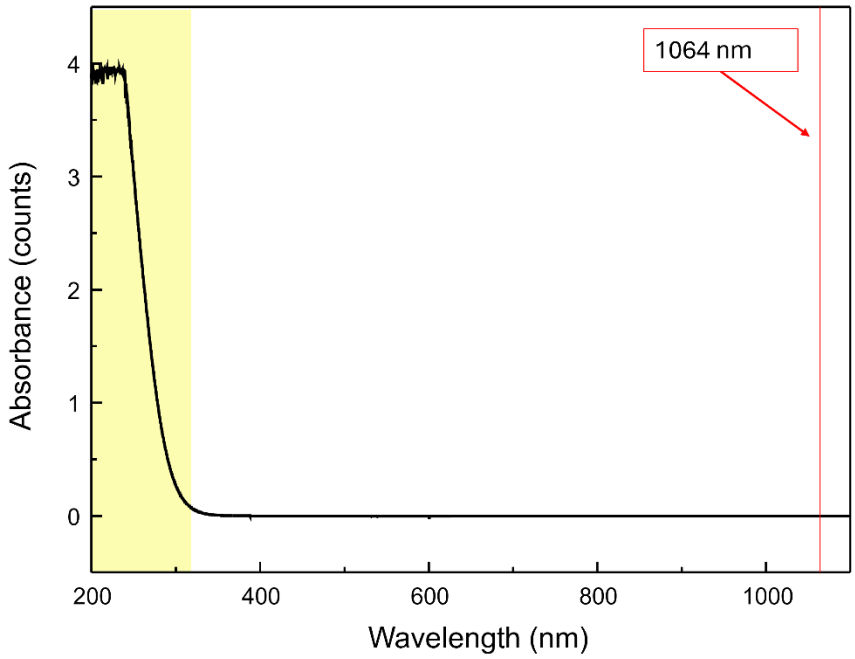

Figure 4. 3 UV-Vis absorption spectrum of the glass window used in our setup.

Figure 4. 4 Picture of the glass with the clear damage caused by the laser.

4.2. Optimization of polyynes production

Once an appropriate design for the recirculation system has been identified, as described in the preceding section, various ablation parameters were tested to optimize the concentration of the produced polyynes. These parameters include the choice of the solvent, the configuration employed, the laser fluence, energy, and spot size. Since in this work every ablation is performed with same volume and duration (100 ml and 90 min), the enhancement in production is equivalent to an increase in polyynes concentration in the final solution. For each ablation, the following data were collected: the target mass loss, measured using a high-precision (i.e., uncertainty of 0.01mg) balance (Radwag), before and after the ablation; UV-Vis absorption spectra of the ablated solutions, extracted every 15 minutes during the 90-minute ablation period; HPLC Chromatogram of the final ablated solution. These last two techniques are used as described in section 3.3. The UV-Vis analysis allows to observe the temporal evolution of polyynes concentration, calculated using Lambert-Beer law. The absorbance to be considered for every polyyne is calculated using the difference in height between the peak and the average of its valleys, to eliminate background contributions. Additionally, HPLC provides a more detailed concentration profile of the different polyynes in the final solutions. Both the characterization techniques use a molar extinction coefficient ε=178000 from the literature [80].

4.2.1. Selection of the solvent

To select the best solvent between methanol and acetonitrile, I conducted three distinct ablations for each solvent varying the laser energy. The setup does not

include a focusing lens, resulting in a non-focused laser beam with a radius of 4.5 mm that remains fixed during the three experiments. The only parameter allowing fluence variation is the laser pulse energy. For methanol, I employed energies of 150, 225, and 300 mJ/pulse, corresponding to fluences of 0.24, 0.36, and 0.48 J/cm², respectively. In the case of ACN, the energies used were 175, 225, and 275 mJ/pulse, corresponding to fluences of 0.28, 0.36, and 0.43 J/cm². The UV-Vis spectra of the final solutions ablated in ACN and MeOH under identical parameters (225 mJ/pulse) are presented in Figure 4. 5. Clearly, the ACN solution exhibits more intense peaks characteristic of polyynes (as listed in Table 3.3) compared to those in MeOH. However, the background in the ACN spectrum is significantly higher. This trend aligns with the results reported by Peggiani et al. [10], as previously described in Section 3.1.2.

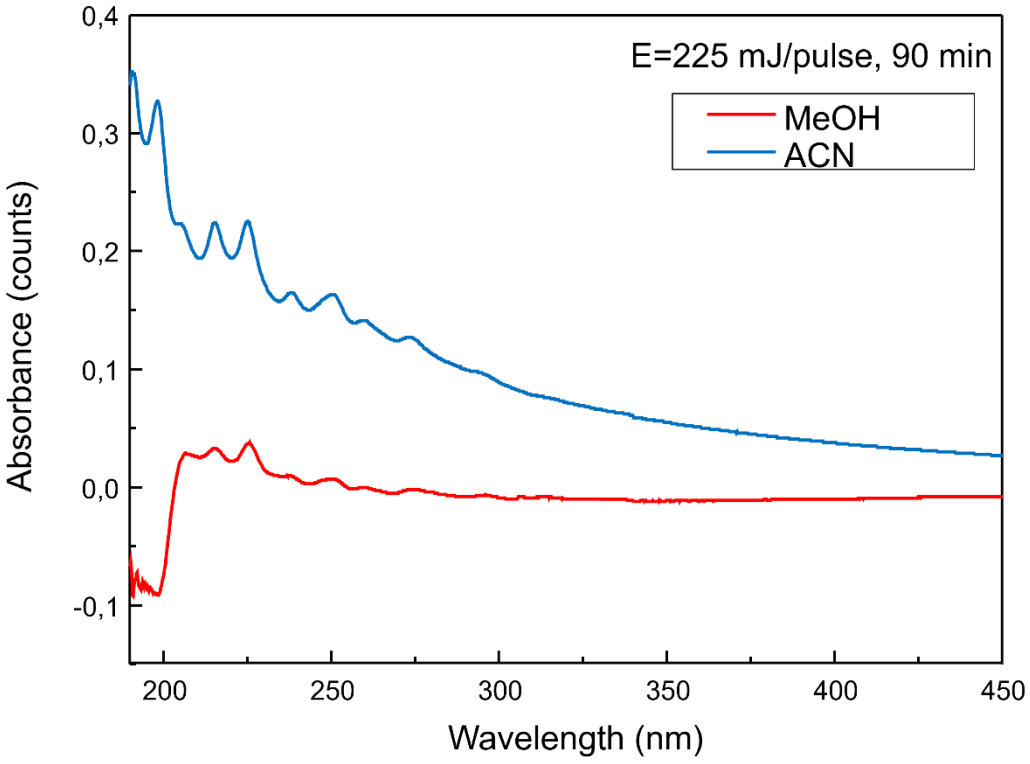

Figure 4. 5 UV-Vis spectra of solutions (diluted 20 times) obtained after 90 min by PLAL in MeOH and in ACN.

Thanks to HPLC analysis, I could observe the concentration trends of polyynes of different lengths in the two solvents. In the obtained chromatograms, polyynes from HC_6H to $HC_{16}H$ are observable in the ACN solution, while those from HC_8H to $HC_{16}H$ are observable in the MeOH solution, because the peak of HC_6H falls within the UV cutoff region of the alcohol. Longer polyynes, like $HC_{18}H$ and $HC_{20}H$, are not visible due to their low concentrations in solution obtained with the low fluences used in these experiments. In Figure 4. 6 and in Figure 4. 7 are represented the concentrations of HC_8H and $HC_{14}H$, respectively, in both solvents for various energies. It is evident that the concentration is always higher for ACN solutions, and it increases with higher energy. For instance, with 225 mJ/pulse, the concentration of HC_8H in ACN is twice that in MeOH. The same trend is also confirmed for longer polyynes (i.e. $HC_{14}H$) Figure 4. 7. Therefore, the use of ACN is advantageous for both short and long polyynes, allowing for a more concentrated solution compared to methanol. Despite its lower index of purity, I selected ACN as the solvent to be used for the upcoming ablations.

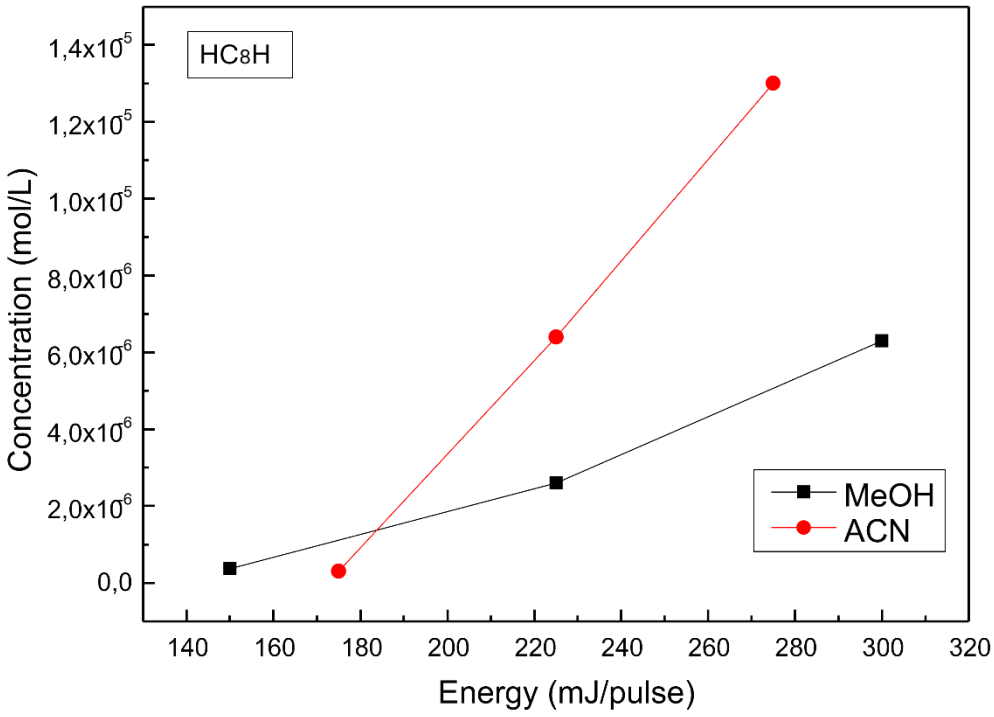

Figure 4. 6 Concentration of HC_8H in solutions obtained by PLAL in MeOH and ACN, with respect to the pulse energy used during the ablations.

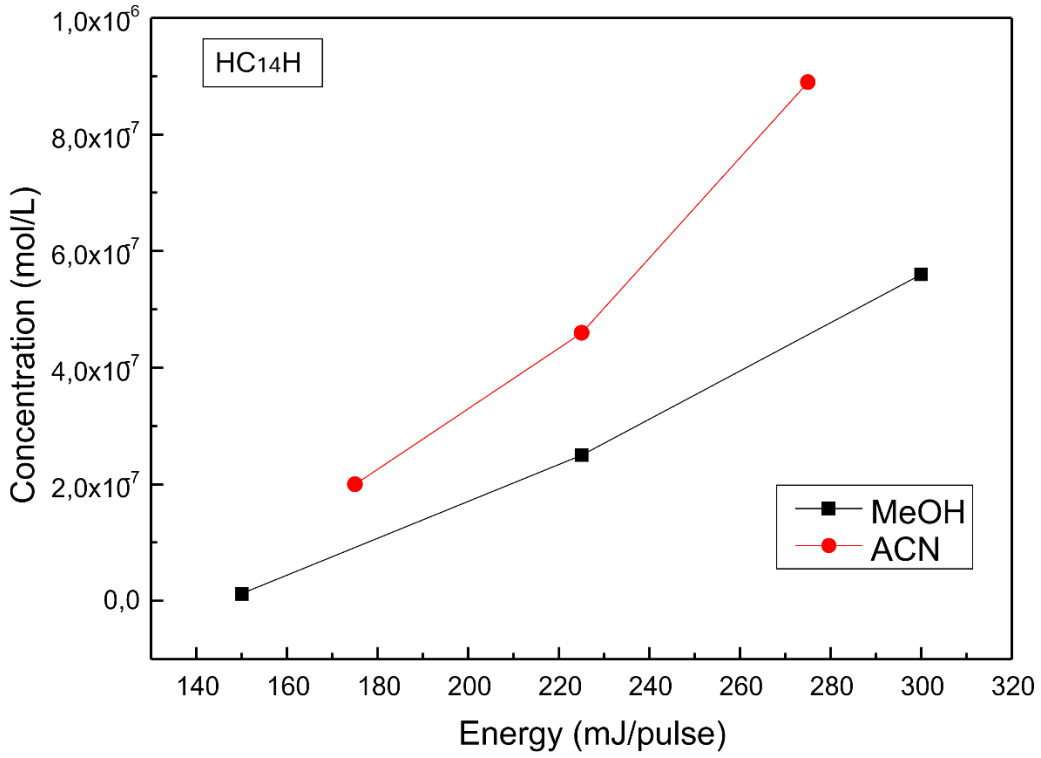

Figure 4. 7 Concentration of $HC_{14}H$ in solutions obtained by PLAL in MeOH and ACN, with respect to the pulse energy used during the ablations.

4.2.2. Selection of the recirculation system configuration

The cell design is fundamental for the ablation process since affects the flow passing through controlling the volume of solution in the ablation site and the amount of energy that hits the target placed inside. Since the cell designed presents removable parts, it can be assembled in different configurations. In my experiments, I used three distinct cell configurations to determine the most suitable configuration for the subsequent experiments. I will refer to the three configurations as: top glass, inside glass, and full cell (see Figure 4. 8). The first one is the standard configuration, where the top and side openings of the cell are sealed with a custom-made glass window cut from a microscope slide (Marienfeld). This arrangement ensures the absence of leakage if the system is not under pressure, as in my experiments. However, due to the cell design and pump limitations, achieving a completely liquid-filled cell is not feasible. Consequently, an air layer above the solvent exists

within the cell, increasing the number of interfaces the laser must traverse before reaching the target.

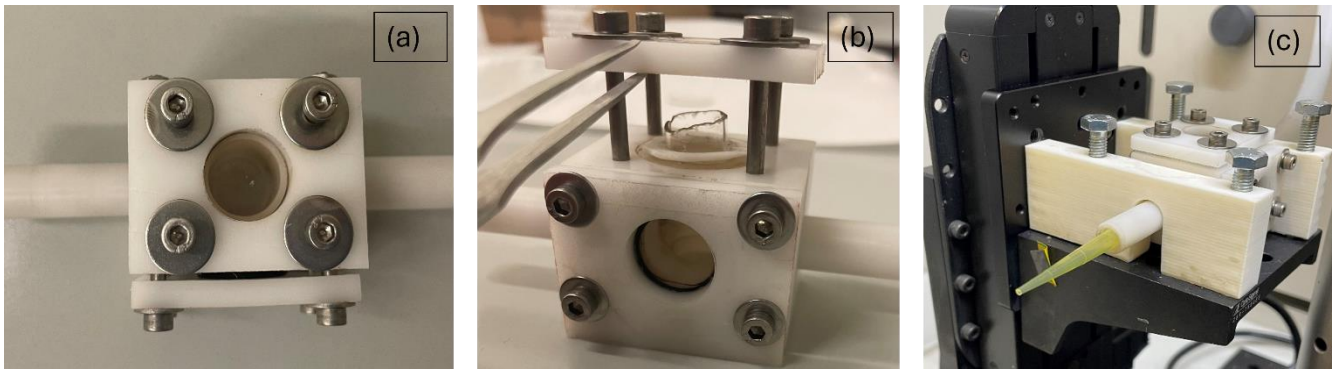

Figure 4. 8 The three cell configurations used in this work: (a) top glass, (b) inside glass, (c) full cell.

In the experiments performed under non-focusing conditions, I employed the top glass configuration. I attempted to use the same configuration with a focused laser to increase fluence, with parameters E=140 mJ/pulse (energy per pulse), r=1.39 mm (spot radius), and F=2.3 J/cm² (fluence). However, at the end of the experiment, the target developed a central hole, as depicted in Figure 4. 9a. Several factors could have contributed to this problem. Among various hypotheses, the most plausible one appears to be related to the deviation and focalization effect of the laser beam due to the presence of a droplet on the glass surface. I experimentally observed this droplet beneath the glass window. It results from solution splashes during ablation that accumulate on the bottom surface of the glass above the target. The curved, lens-like surface of the droplet, along with the refractive index variation at the interface between the liquid and air, can cause the laser beam to focus on the focal centre of the droplet, as illustrated in Figure 4. 10. According to my hypothesis, this phenomenon cancels the effect of the stage movement, assuming that the droplet and target are not moving with each other. Consequently, the focused laser continuously deviates toward the fixed focal centre of the droplet, leading to excessive consumption of the target material at that point, eventually resulting in a hole. This situation occurs in the top glass configuration, as confirmed also in other ablations using a non-focused laser, where one or more spots on the target exhibit significantly higher consumption at the end of the ablation, as shown in **Errore. L'origine riferimento non è stata trovata.**b. Given the uncontrollable nature of the system, I have designed two possibilities to avoid such droplets: the inside glass and full cell configurations.

In the inside glass configuration (see Figure 4. 8b), I designed a glass window with a ‘tube shape’ that can be inserted into the cell at an adjustable height for each

experiment. The lower glass surface, which enters the cell, must be positioned in contact with the liquid surface to allow unimpeded flow. However, the placement should not be too close to the target, as it could interfere with the plasma zone during ablation.

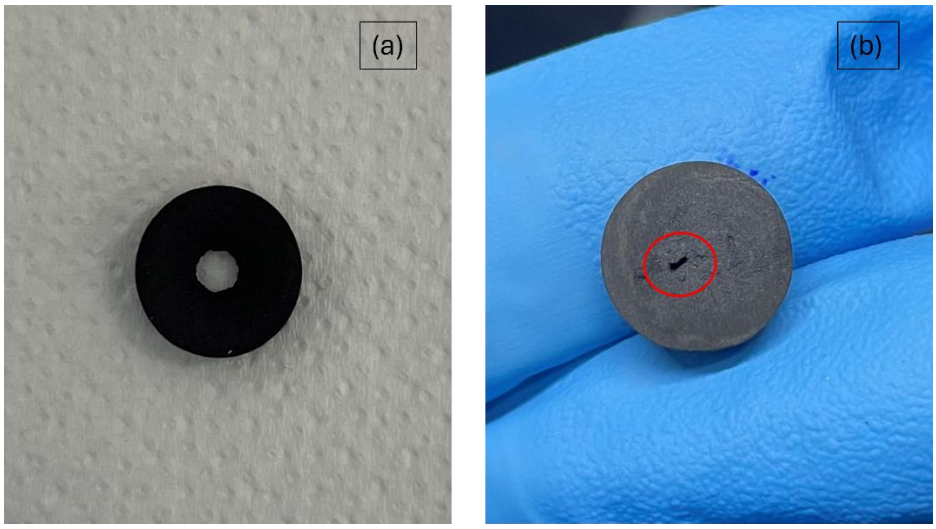

Figure 4. 9 Pictures of (a) the drilled target, and (b) the target with a surface hole.

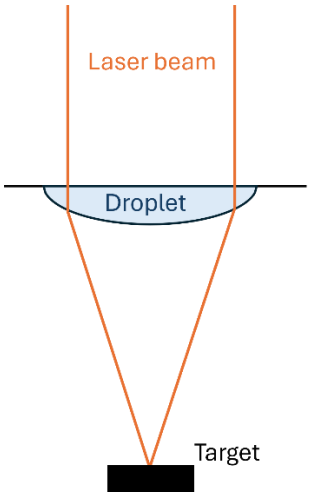

Figure 4. 10 Sketch of the hypothesized focusing process by a droplet.

By using the inside glass configuration, it was possible to ablate both with focused and unfocused laser beams. In the case of the unfocused laser, the same parameters as in the top glass configuration was used for comparison. In Figure 4. 11 the UV-vis spectra obtained from ablations with the non-focused laser at 275 mJ/pulse in

the two different configurations is shown. The spectrum for the inside glass arrangement exhibits characteristic peaks of the polyynes much lower than the other, along with a lower background. This suggests that the target was ablated less. Probably because in the case of top glass, the focusing phenomenon described earlier occurs, resulting in a higher effective fluence reaching the target, even though it is not directly calculable. **Errore. L'origine riferimento non è stata trovata.** corresponds to this ablation and confirms that the target was preferentially consumed in a precise spot, much smaller than the diameter of the laser beam. Through HPLC analysis of the two solutions, I obtained polyynes concentrations nearly an order of magnitude higher in the top glass case. As an example, the concentration of HC_8H was 1.3×10^{-5} mol/L in the top glass configuration, compared to 2.9×10^{-6} mol/L in the inside glass case. Despite the lower concentration, this latter configuration provides the advantage of uniform target consumption, avoiding the risk of perforating the target.

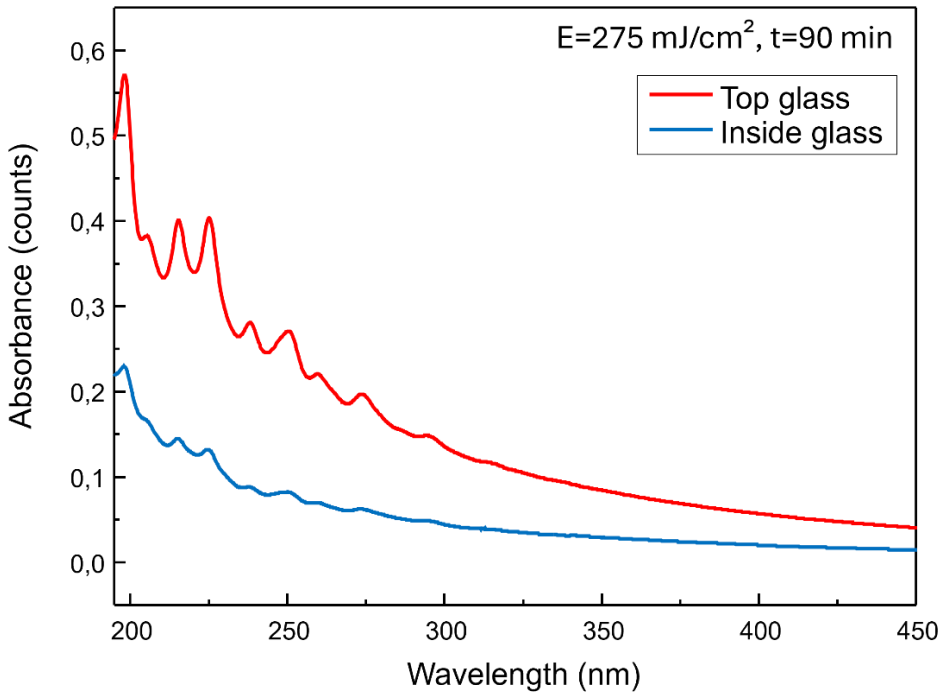

Figure 4. 11 UV-Vis spectra of two solutions obtained by PLAL in ACN through a recirculation system in two different configurations. The unfocused laser energy was 275 mJ/pulse and ablation time 90 min.

Instead in the case of focused laser for the inside glass configuration, the parameters used were: 0.76 mm of spot radius, 40 mJ/pulse of energy, and 2.16 J/cm² of fluence. Initially, the glass bottom was in contact with the solvent flowing inside the cell,

positioned approximately 5 mm above the target. However, during the ablation process, I observed a gradual decrease in the liquid level within the cell. This phenomenon is likely due to the ablation gases moving upward, accumulating beneath the glass and creating pressure that lowers the liquid layer. Probably in the case of unfocused laser at 275 mJ/pulse this decrease was less evident because of the lower fluence used that can lead to a lower production of ablation gases. Although the inside glass configuration can be partially controlled by periodically adjusting the pump parameters, it still provides limited variation due to the approximately 5 mm gap between the target and the glass. The ablation results were not promising for this configuration. For instance, through HPLC analysis, I obtained a concentration of HC_8H of 5.6×10^{-6} mol/L, which is low considering the laser parameters used. Possible explanations for this outcome include an excessively thin liquid layer, preventing optimal plasma expansion and confinement, or irregularities caused by the glass piece inserted into the cell, such as flow variations or turbulences. However also using a focused laser this configuration ensures a proper consumption of the target, that follows the circulation motion of the stage. Consequently, I developed a design that allows the liquid to be in contact with the glass but also providing a greater margin for the liquid layer height variations, that is the full cell configuration.

The full cell (see Figure 4. 8c) is similar to the first one, featuring the standard glass window on top of the cell, but it includes an additional constriction at the outlet (i.e., reduced section of the outlet) that leads to a reduction of velocity of the outgoing flow and allowing for complete cell filling. An ablation performed in this configuration with E = 90 mJ/pulse, r = 1.45 mm, and F = 1.35 J/cm² resulted in a solution with an HC_8H concentration of 1.3×10^{-5} mol/L. Due to the variation in different parameters, it is not directly comparable to the ablation described above at a fluence of 2.16 J/cm². Neverthless, despite the reduction in fluence, a higher concentration of polyynes was obtained. This increase could be attributed to both the different configuration used and the larger spot size (from a radius of 0.766 mm to 1.45 mm), resulting in a greater ablated target surface. However, the reduction in the liquid layer height is less critical in this configuration, thanks to the initial greater distance between the liquid surface and the target. By periodically adjusting the pump parameters, it becomes easier to maintain the liquid in contact with the glass. In this case as well, target consumption remains uniform. Therefore, this configuration is more reliable and controllable, making it the chosen setup for investigating the laser parameter effects on polyynes production.

4.2.3. Optimization of laser parameters

In this section, I will show how the production of polyynes changes based on the laser parameters used for ablations with the full cell configuration. As described in section 2.3.2, the work of Marabotti et al. [59] investigates the relationship between polyynes concentration and laser parameters in the batch configuration. Therefore, I have taken their results as a starting point for my exploration. In their work is highlighted that the concentration depends on both fluence and spot radius. With the fluence, the energy intensity on the target surface can be increased, while with the spot radius, the ablation area can be enlarged. A series of ablations were performed gradually increasing the spot size from 0.76 mm to 1.45 mm and 1.8 mm in radius, while keeping the fluence constant at 1.35 J/cm², thanks to a gradual increase of the pulse energy. For each spot size showing an increase in concentration, the fluence was changed between 1.8 and 2.2 J/cm², remaining within safe conditions relative to the threshold for glass damage. For the best result, which was achieved with a radius of 1.8 mm and fluence of 2.2 J/cm², a further increase in the radius (i.e., 2.0 mm) was tested. In this last experiment, the stage was set to its maximum height reaching the larger spot size available with the setup used in this work. It is known that a portion of the laser is always reflected during ablation. The reflection angle depends on the incident angle with which the laser hit the reflective surface - that could be both the glass and the liquid surface. The laser does not hit the surfaces at 90 ° since in this setup the mirrors was slightly rotated to avoid the reflection to go back inside the laser, which could damage the laser itself. When the cell is positioned close to the focusing lens (as in the case of the 2.0 mm radius), the reflection can hit the lens causing a damage. Thus, the cell was tilted by 2.5° to increase the angle of reflection relative to the vertical avoiding hitting the focusing lens. In Figure 4. 12 the results obtained from ablations at different fluences, and spot sizes are summarized.

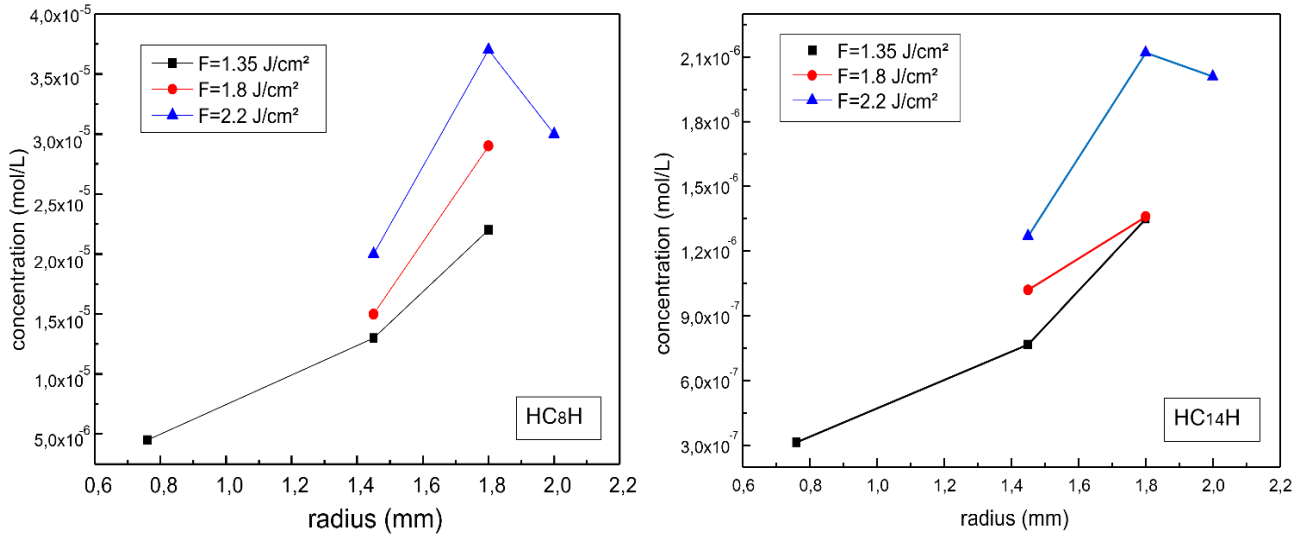

Figure 4. 12 Plot of HC_8H and $HC_{14}H$ concentration as a function of the spot radius for ablated solutions obtained at different fluences.

It is evident that the concentration of both short (HC_8H) and long ($HC_{14}H$) polyynes increases with the spot radius and fluence, up to a radius of 1.8 mm and 2.25 J/cm² of fluence, corresponding to the maximum concentration obtained. This effect is more pronounced when increasing the radius instead of fluence. Passing from a radius of 1.45 mm to 1.8 mm (a 24% increase) at a fluence of 1.8 J/cm², the concentration of HC_8H rises from 1.5 × 10^{-5} mol/L to 2.9 × 10^{-5} mol/L (a 90% increase). Instead, when increasing the fluence from 1.35 J/cm² to 1.8 J/cm² (a 30% increase) at a radius of 1.8 mm, the HC_8H concentration increases by 30%, from 2.2 × 10^{-5} mol/L to 2.9 × 10^{-5} mol/L. This trend is plausible because a linear increase in radius results in a quadratic increase in the spot size, i.e., the ablated surface area. However, larger spot sizes lead to a greater volume of 'polyynes destruction'. The polyynes contained in this region are irradiated by the incoming laser and they can be degraded by the strong energy of the laser. Furthermore, for keeping the fluence constant while the spot size is increasing, also the energy needs to be increased. Thus, polyynes production becomes a compromise between creation and destruction. This increase in irradiated volume and laser energy may explain the reduction in both short and long polyynes concentration observed when the radius was increased from 1.8 mm to 2.0 mm and the energy from 230 mJ/pulse to 280 mJ/pulse, to keep the fluence constant at 2.2 J/cm².

For each ablation, the mass of the target before and after the process was measured, allowing to calculate the mass loss corresponding to the ablated material. As shown

in Figure 4. 13, the mass loss increases with both the radius and the fluence, similarly to the trend of polyynes concentration. However, there is a noticeable difference between the two trends when transitioning from a radius of 1.8 to 2.0 mm. In this range, the concentration decreases, but the mass loss increases. This discrepancy strengthens my hypothesis: having a greater ablated mass and a lower concentration of polyynes implies that some of them are either not formed or are destroyed. However, this remains only a hypothesis, because the ablations are non-replicable processes and small differences in results are expected, and the measurement of mass loss inherently carries uncertainties. Due to reaching a limit condition for my setup, I was unable to further investigate the inversion in polyynes concentration observed in Figure 4. 12.

In conclusion the investigation on the optimal parameters gave as best result a spot size of 1.8 mm and a fluence of 2.25 J/cm^2, that allows to obtain the maximum concentration of polyynes (i.e., 4,93 x 10^{-5} mol/L of HC_6H; 3,71 x 10^{-5} mol/L of HC_8H; and 2,12 x 10^{-6} mol/L of $HC_{14}H$) with a target consumption of 10.5 mg.

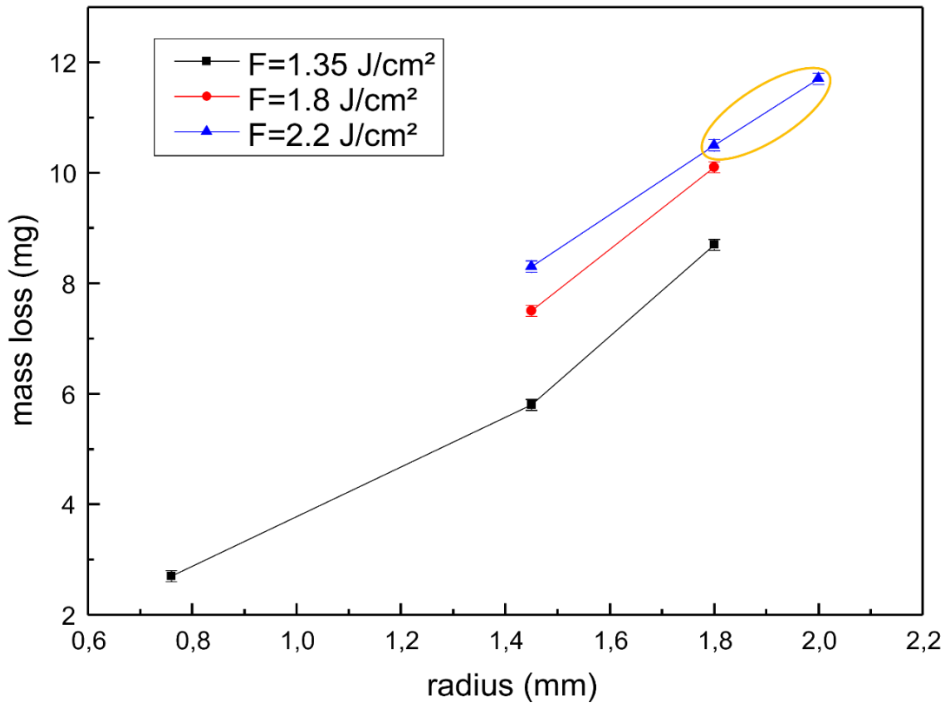

Figure 4. 13 Mass loss during the ablations in function of the spot radius and fluence used.

4.3. Comparison between static and recirculation production of CAWs by Pulsed Laser Ablation in Liquid

In this paragraph, I will compare an ablation performed in static production configuration with the ablation described in section 4.2.3, which was conducted under recirculation production conditions, both using the same parameters. The laser employed had an energy of 230 mJ/pulse, a spot radius of 1.8 mm, and a fluence of 2.2 J/cm². As in the other ablations, the volume of ACN was 100 ml, and the duration was 90 minutes. In the batch configuration, the solvent height above the target was approximately 5 cm, whereas in the flow cell conditions, it was 1.7 cm. The results obtained from the two ablations are depicted in Figure 4. 14 where the concentrations of polyynes are plotted as a function of their length.

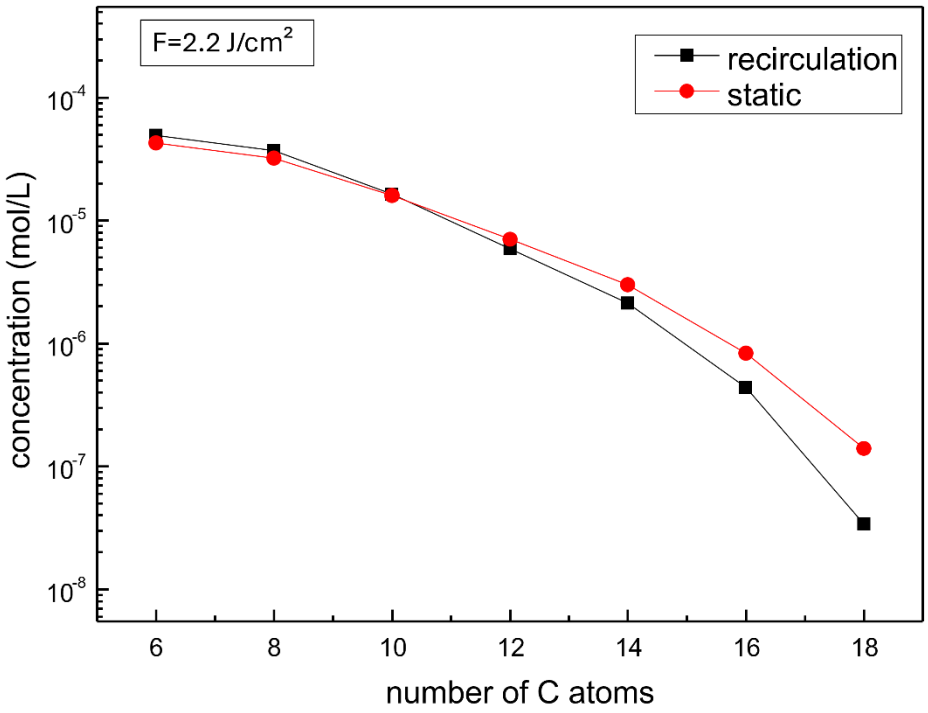

Figure 4. 14 Plot of polyynes concentration obtained by PLAL in static and recirculation mode, as a function of the number of carbon atoms for each polyyne.

In both cases, as expected, the concentration decreases with an increase in the number of sp-carbon atoms, corresponding to the chain length. As explained in

section 2.3.1, the formation of polyynes is governed by two processes: chain growth and termination. Through this mechanism, it is easier to obtain shorter chains compared to longer ones, resulting in consistently lower concentrations of longer chains. Comparing the two different production methods, in the recirculation case, shorter polyynes are more concentrated than in the static case. For example, for HC_6H, the concentration increases by 15%, from 4.27×10^{-5} mol/L to 4.93×10^{-5} mol/L. Similarly, for HC_8H, there is an increase of 15%, from 3.22×10^{-5} mol/L to 3.71×10^{-5} mol/L. Instead, for longer polyynes (from 12 sp-carbon atoms onwards), the static system provides higher concentrations. For instance, in the case of $HC_{16}H$, the static mode yields a polyyne concentration of 8.34×10^{-7} mol/L, almost double that obtained in the recirculation system (4.38×10^{-7} mol/L). This inversion of the production trend for polyynes is not well understood and is challenging to explain due to the rapid process times. One possible hypothesis relates to liquid flow, which could alter plasma dynamics or reduce the concentration of radical species, such as C_2, within the plasma, thereby limiting chain growth. Even for short polyynes the results obtained are not as expected. Indeed, the advantage provided by the recirculation system appears to be rather low. As explained in section 2.2.1, considering the liquid flow, which transports ablated material and impurities away from the ablation site, along with a significant reduction in the liquid layer height above the target, the laser should strike the target with greater energy, thereby increasing polyynes production. However, it's likely that this system does not ensure an appropriate laminar flow to perform these functions effectively.

Another expected difference should be on the time evolution of polyynes concentration, that is represented in Figure 4. 15. The time evolution was made possible through characterization using UV-Vis spectroscopy every 15 minutes. The results obtained slightly differ from those calculated before based on HPLC analysis and are less reliable. However, in this context, they serve to describe the temporal trends rather than the final concentrations (which were previously described). Throughout the entire ablation duration (90 minutes), the concentration of polyynes continues to increase over time, both in the static and recirculation cases. In both scenarios, the concentration increase is highest at the beginning and decreases toward the end of ablation, approximately after 60 minutes. For instance, in the static case, the relative concentration of HC_8H increases by 90% in the range between 15 and 30 minutes (from 5.3×10^{-6} mol/L to 1.01×10^{-5}mol/L), and by 6% in the last 15 minutes of ablation (from 2.01×10^{-5} mol/L to 2.14×10^{-5}mol/L). Meanwhile, in the recirculation case for the same time intervals the relative increase is 71% at the beginning, and 8% at the end of ablation. This decreasing trend in concentration increment over time is more pronounced in the static case. Various factors may contribute, such as reaching a too concentrated solution where

polyynes interact through cross-linking phenomena or the presence of a high quantity of byproducts and impurities leading to an increased laser absorption, effectively masking the target and reducing energy delivery.

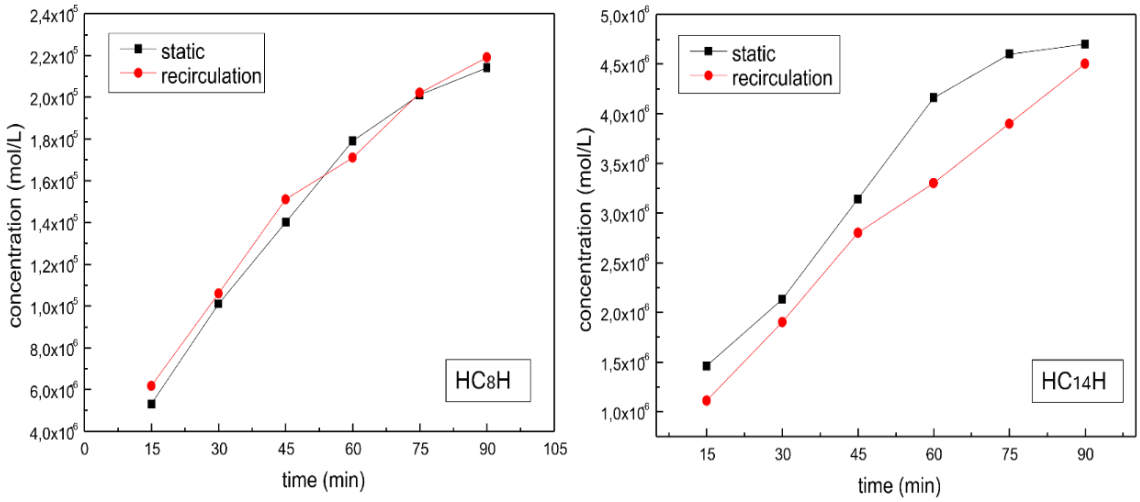

Figure 4. 15 Time evolution of HC_8H and $HC_{14}H$ concentration during the ablation in both static and recirculation mode. The concentrations are obtained by Lambert-Beer law based on the UV-Vis results.

To better observe the differences in the two trends, I calculated the average production rates for each 15-minute interval by dividing the concentration increment by the time interval and multiplying it by the total volume, thus obtaining the increase in polyynes quantity over time. The results are presented in Figure 4. 16, where each marked time represents the interval between that time and the one before it. Notably, the production rates generally exhibit a decreasing trend. In the last 45 minutes, it is evident that the production rate decreases much faster in the static case compared to the recirculation case, both for shorter and longer polyynes. Specifically, the production rates reach very low values: 8.67×10^{-9} mol/min for HC_8H and 6.67×10^{-10} mol/min for $HC_{14}H$ in the static case. Meanwhile, in the recirculation case, I observed a more gradual decrease, and for the longer polyynes, there appears to be a stabilization around 4.0×10^{-9} mol/min. This difference in trend may be attributed to several beneficial factors associated with the recirculation production. However, due to the limited reproducibility of ablations, a more detailed analysis with repeated experiments would be necessary to draw appropriate conclusions. One advantage that may have contributed is the reduced liquid height in the cell compared to the static ablation chamber. In both configurations, as the ablation time progresses, the solution becomes increasingly

concentrated in both polyynes and byproducts. However, in the beaker case, the volume through which the laser must pass to hit the target is much larger, leading to more frequent absorption and scattering phenomena. Consequently, the masking effect in the cell is likely less pronounced, aided by the flow that removes particles and cavitation bubbles formed at the ablation site. Despite this, the advantage related to flow does not appear as evident from the final concentrations obtained in my experiments, indicating that flow optimization will be necessary.

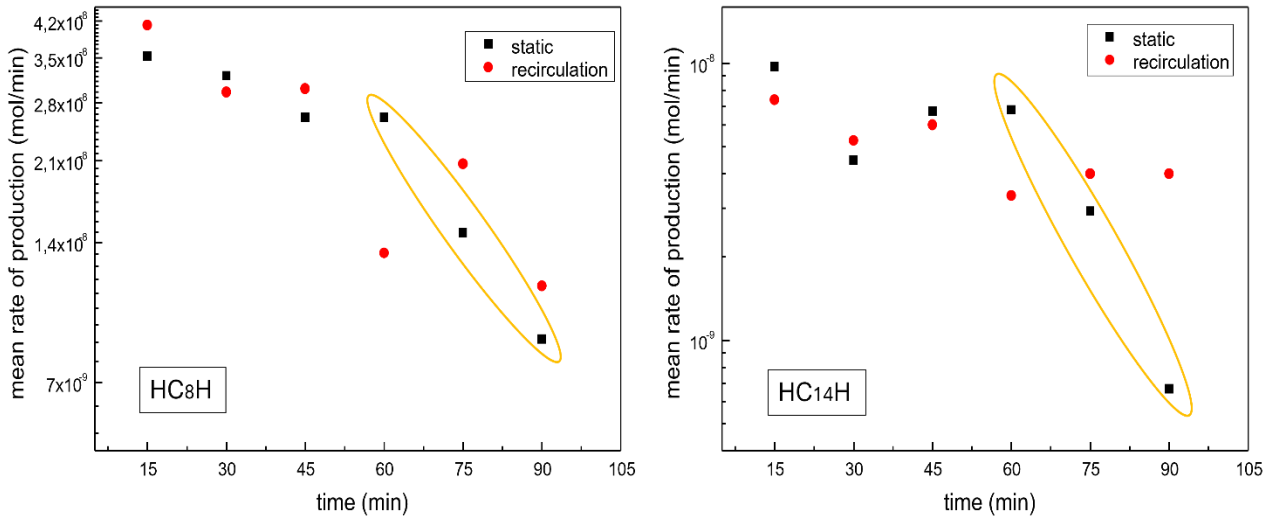

Figure 4. 16 Logarithmic plot of the mean rate of production for HC_8H and $HC_{14}H$ as a function of ablation time. It is calculated each 15-minutes interval based on the concentrations presented in Figure 4. 15.

A result that appears incongruent with these hypotheses is the target consumption, which is higher in the static case with a mass loss of 11.7 mg compared to the 10.5 mg in the recirculation case. In static conditions, one would expect less energy to reach the target due to the masking effect, resulting in lower target consumption. However, the target consumption in the nanosecond laser conditions also depends on thermal factors. The target in the flow cell is constantly cooled by the liquid flow, which could reduce the target consumption. Additionally, I calculated the mass of the various polyynes detectable by HPLC by multiplying the molar mass of each polyyne by its quantity in solution. Summing up all contributions I obtained the total mass of polyynes in solution, excluding uncharacterized polyynes such as C_2 and C_4 (which fall within the solvent cutoff) and longer polyynes beyond $HC_{18}H$ due to their very low concentrations and impossibilities to be detected with HPLC. In the recirculation case, the percentage of total polyynes mass (1.04 mg) relative to

mass loss is 9.9%, while in the static system, the total mass is 0.98 mg, resulting in an 8.4% of the mass loss. Thus, it appears that recirculation production exhibits greater efficiency in generating polyynes from the ablated mass. However, as previously mentioned, assumptions regarding mass loss would require more detailed studies due to measurement instability and limited reproducibility of the ablation.

Despite the unexpected lack of increased production, the recirculation system has confirmed several significant advantages. The use of an ablation cell, instead of a static ablation chamber, allows for spatial separation of the ablation site and solution storage, providing an additional degree of freedom to the system. For instance, in the recirculation production, I can increase the total volume of solvent to be ablated without needing to enlarge the volume within the ablation site, thus maintaining the liquid height above the target. Another promising result for the future is the advantage observed in terms of production rates, suggesting that longer ablation times could yield greater productivity gains compared to the static case. Additionally, the recirculation system enhances safety during ablation. The cell operates in a more closed configuration, with less oxygen volume at the ablation site, thereby reducing the risk of ignition and fires. Consequently, it enables high-energy ablations that would be dangerous in the static system.

5 Conclusions and future perspectives

The purpose of this thesis was to optimize the production of polyynes by PLAL using a novel recirculation method. The optimization process involved two main aspects: (i) designing an optimal recirculation system and (i) fine-tuning the ablation process parameters. The results obtained demonstrate that it is possible to increase the concentration of polyynes produced via PLAL in the recirculation mode by adjusting the laser parameters, such as laser fluence and spot radius. For instance, in the ablations conducted, the maximum concentrations achieved were 4.93×10^{-5} mol/l for HC_6H and 3.71×10^{-5} mol/l for HC_8H in 100 ml of ACN, using a laser with an energy of 230 mJ/pulse and a spot radius of 1.8 mm, corresponding to a fluence of 2.25 J/cm^2. In the static case, using the same parameters, I obtained slightly lower concentrations of short polyynes, such as 4.27×10^{-5} mol/L of HC_6H, and higher concentrations of longer polyynes, such as 8.34×10^{-7} mol/L of $HC_{16}H$, compared to 4.38×10^{-7} mol/L in the recirculation case. However, the increase in production of short polyynes is not that significant, and some concentration variations may also be attributed to the limited reproducibility of ablations. The most promising result from the recirculation system regards the production rate. I demonstrated that the rate of production decreases less over time in the recirculation case compared to the static one. Specifically, in the last 15 minutes of ablation, the production rates were higher in recirculation production: 1.13×10^{-7} mol/min for HC_8H and 4.0×10^{-9} mol/min for $HC_{14}H$, with respect to 8.67×10^{-8} mol/min and 6.67×10^{-10} mol/min obtained in batch production, respectively. This advantage of the recirculation production is crucial for scaling up the process. If the production rate does not decrease a lot over time, longer ablation times can be employed to continue producing significant quantities of polyynes. Another important benefit of this method lies in the decoupling of the ablation site volume and the total volume to be ablated. Thus, it is possible to significantly increase the ablation volume

without raising the liquid column above the target, that is responsible of absorption and scattering phenomena. Additionally, the recirculation system enhances safety. Unlike the static ablation chamber, which carries a high risk of ignition for high laser energies due to its open configuration, the cell operates in a more closed environment with less oxygen at the ablation site. Consequently, it enables high-energy ablations that would be hazardous in the static system.

Therefore, the recirculation system I have created still needs to be implemented to achieve greater advantages compared to the static system. Optimization of solvent flow will be necessary, achieved through suitable design and flow parameters to maintain laminar flow conditions and an optimal volume within the cell. It is hoped that through this optimization, we can derive maximum benefit from the recirculation system, as demonstrated in literature for nanoparticle production. For the system I have developed, a more pronounced advantage over the static case could likely be observed by increasing the volume and duration of ablation. As explained earlier, the advantage in production rates with recirculation suggests this approach. Probably, in the static case, increasing the volume would result in a much greater decrease in productivity compared to the recirculation system, where the volume within the ablation site remains constant. For ablations with very large volumes of solvent, on the order of liters, a sustainable future perspective would be the integration of a system that allows for polyynes concentration and solvent purification for reuse in other ablations, such as with a rotavapor. Another crucial factor that can impact polyynes productivity is the purity of the solution within the ablation site. In fact, the production rate should be higher in a solution with fewer impurities and byproducts. Therefore, implementing a filtration system that acts on the recirculating fluid, removing impurities (e.g., ablation byproducts) that the filter can retain, would allow for a cleaner solution that absorbs less laser energy. Another possibility could be to collect polyynes during recirculation, away from the ablation site. This way, a smaller amount of polyynes would be degraded at the ablation site due to laser energy. I have devised a potential system for accumulating polyynes using two solvents to be implemented in the recirculation process. These two solvents are contained in the beaker and must be immiscible, forming two separate phases. The lighter phase, which sits on top, should be nonpolar and is referred to as the stationary phase (for example, cyclohexane). The phase below it is the mobile phase, which is recirculated and ablated in the flow cell (for example, ACN). Due to the difference in polarity, polyynes tend to stay in the nonpolar stationary phase. Through an extraction process, they should transfer from ACN to cyclohexane. However, polyynes extraction efficiency

depends on several parameters, so investigating optimal conditions to maximize it will be necessary. This biphasic system would allow us to shift the balance between polyynes degradation and creation at the ablation site, potentially leading to increased polyynes production.

Bibliography

[1] C. S. Casari, M. Tommasini, R. R. Tykwinski, and A. Milani, "Carbon-atom wires: 1-D systems with tunable properties," *Nanoscale*, vol. 8, no. 8. Royal Society of Chemistry, pp. 4414–4435, Feb. 28, 2016. doi: 10.1039/c5nr06175j.

[2] C. S. Casari and A. Milani, "Carbyne: from the elusive allotrope to stable carbon atom wires," *MRS Commun*, vol. 8, no. 2, pp. 207–219, 2018, doi: DOI: 10.1557/mrc.2018.48.

[3] A. L. K. Shi Shun and R. R. Tykwinski, "Synthesis of naturally occurring polyynes," *Angewandte Chemie - International Edition*, vol. 45, no. 7. 2006. doi: 10.1002/anie.200502071.

[4] H. W. Kroto, J. R. Heath, S. C. O'Brien, R. F. Curl, and R. E. Smalley, "C60: Buckminsterfullerene," *Nature*, vol. 318, no. 6042, pp. 162–163, 1985, doi: 10.1038/318162a0.

[5] A. Hirsch, "The era of carbon allotropes," *Nature Materials*. Nature Publishing Group, pp. 162–163, 2010. doi: 10.1038/nmat2885.

[6] C. S. Casari, "Carbon atomic wires: from stars to nanotechnology," 2012. doi: http://dx.doi.org/10.4081/scie.2012.130.

[7] A. Milani, A. Li Bassi, V. Russo, M. Tommasini, and C. S. Casari, "Linear Carbon: From 1D Carbyne to 2D Hybrid sp-sp2 Nanostructures Beyond Graphene," in *Handbook of Graphene, Volume 3: Graphene-Like 2D Materials*, vol. 3, 2019, pp. 297–340. Accessed: Feb. 11, 2024. [Online]. Available: https://hdl.handle.net/11311/1095289

[8] Y. Gao, Y. Hou, F. Gordillo Gámez, M. J. Ferguson, J. Casado, and R. R. Tykwinski, "The loss of endgroup effects in long pyridyl-endcapped oligoynes on the way to carbyne," *Nat Chem*, vol. 12, no. 12, pp. 1143–1149, 2020, doi: 10.1038/s41557-020-0550-0.

[9] A. Milani *et al.*, "Raman spectroscopy as a tool to investigate the structure and electronic properties of carbon-atom wires," *Beilstein Journal of Nanotechnology*, vol. 6, no. 1, pp. 480–491, 2015, doi: 10.3762/bjnano.6.49.

[10] S. Peggiani *et al.*, "Solvent-dependent termination, size and stability in polyynes synthesized: Via laser ablation in liquids," *Physical Chemistry*

Chemical Physics, vol. 22, no. 45, pp. 26312–26321, Dec. 2020, doi: 10.1039/d0cp04132g.

[11] T. Wakabayashi, M. Saikawa, Y. Wada, and T. Minematsu, "Isotope scrambling in the formation of cyanopolyynes by laser ablation of carbon particles in liquid acetonitrile," in *Carbon*, 2012. doi: 10.1016/j.carbon.2011.07.053.

[12] S. Szafert and J. A. Gladysz, "Update 1 of: Carbon in One Dimension: Structural Analysis of the Higher Conjugated Polyynes," *Chem Rev*, vol. 106, no. 11, pp. PR1–PR33, Nov. 2006, doi: 10.1021/cr068016g.

[13] W. A. Chalifoux and R. R. Tykwinski, "Synthesis of polyynes to model the sp-carbon allotrope carbyne," *Nat Chem*, vol. 2, no. 11, pp. 967–971, 2010, doi: 10.1038/nchem.828.

[14] L. Shi *et al.*, "Confined linear carbon chains as a route to bulk carbyne," *Nat Mater*, vol. 15, no. 6, 2016, doi: 10.1038/nmat4617.

[15] F. Cataldo, "Polyynes production in a solvent-submerged electric arc between graphite electrodes. III. Chemical reactivity and stability toward air, ozone, and light," *Fullerenes Nanotubes and Carbon Nanostructures*, vol. 12, no. 3, 2004, doi: 10.1081/FST-200026951.

[16] C. W. Patrick, Y. Gao, P. Gupta, A. L. Thompson, A. W. Parker, and H. L. Anderson, "Masked alkynes for synthesis of threaded carbon chains," *Nat Chem*, vol. 16, no. 2, pp. 193–200, 2024, doi: 10.1038/s41557-023-01374-z.

[17] A. Arora, S. D. Baksi, N. Weisbach, H. Amini, N. Bhuvanesh, and J. A. Gladysz, "Monodisperse Molecular Models for the sp Carbon Allotrope Carbyne; Syntheses, Structures, and Properties of Diplatinum Polyynediyl Complexes with PtC20Pt to PtC52Pt Linkages," *ACS Cent Sci*, vol. 9, no. 12, pp. 2225–2240, Dec. 2023, doi: 10.1021/acscentsci.3c01090.

[18] F. Cataldo, "Synthesis of polyynes in a submerged electric arc in organic solvents," *Carbon N Y*, vol. 42, no. 1, 2004, doi: 10.1016/j.carbon.2003.10.016.

[19] S. Peggiani *et al.*, "Size-selected polyynes synthesised by submerged arc discharge in water," *Chem Phys Lett*, vol. 740, 2020, doi: 10.1016/j.cplett.2019.137054.

[20] M. Picollo, M. Aceto, and T. Vitorino, "UV-Vis spectroscopy," *Physical Sciences Reviews*, vol. 4, no. 4, 2019, doi: 10.1515/psr-2018-0008.

[21] H. Tabata, M. Fujii, S. Hayashi, T. Doi, and T. Wakabayashi, "Raman and surface-enhanced Raman scattering of a series of size-separated polyynes," *Carbon N Y*, vol. 44, no. 15, 2006, doi: 10.1016/j.carbon.2006.07.004.

[22] F. Cataldo *et al.*, "Synthesis, Characterization, and Modeling of Naphthyl-Terminated sp Carbon Chains: Dinaphthylpolyynes," *J Phys Chem B*, vol. 114, no. 46, pp. 14834–14841, Nov. 2010, doi: 10.1021/jp104863v.

[23] T. D. Lee, "Introduction to Modern Liquid Chromatography, Third Edition," *J Am Soc Mass Spectrom*, vol. 22, no. 1, 2011, doi: 10.1007/s13361-010-0021-8.

[24] "Basic Concepts and the Control of Separation," in *Introduction to Modern Liquid Chromatography*, 2010. doi: 10.1002/9780470508183.ch2.

[25] F. Cataldo, O. Ursini, G. Angelini, M. Tommasini, and C. Casari, "Simple synthesis of α,ω-diarylpolyynes part 1: Diphenylpolyynes," *Journal of Macromolecular Science, Part A: Pure and Applied Chemistry*, vol. 47, no. 8, 2010, doi: 10.1080/10601325.2010.491749.

[26] A. Ramadhan *et al.*, "Synthesis of hydrogen- and methyl-capped long-chain polyynes by intense ultrashort laser pulse irradiation of toluene," *Carbon N Y*, vol. 118, 2017, doi: 10.1016/j.carbon.2017.03.096.

[27] R. R. Jones, D. C. Hooper, L. Zhang, D. Wolverson, and V. K. Valev, "Raman Techniques: Fundamentals and Frontiers," *Nanoscale Res Lett*, vol. 14, no. 1, p. 231, 2019, doi: 10.1186/s11671-019-3039-2.

[28] Z. Li, L. Deng, I. A. Kinloch, and R. J. Young, "Raman spectroscopy of carbon materials and their composites: Graphene, nanotubes and fibres," *Progress in Materials Science*, vol. 135. 2023. doi: 10.1016/j.pmatsci.2023.101089.

[29] R. S. Tobias, "Raman spectroscopy in inorganic chemistry," *J Chem Educ*, vol. 44, no. 2, 1967, doi: 10.1021/ed044p70.

[30] C. S. Casari *et al.*, "Stabilization of linear carbon structures in a solid Ag nanoparticle assembly," *Appl Phys Lett*, vol. 90, no. 1, 2007, doi: 10.1063/1.2430676.

[31] S. Okada, M. Fujii, and S. Hayashi, “Immobilization of polyynes adsorbed on Ag nanoparticle aggregates into poly(vinyl alcohol) films,” *Carbon N Y*, vol. 49, no. 14, 2011, doi: 10.1016/j.carbon.2011.06.074.

[32] V. Amendola and M. Meneghetti, “What controls the composition and the structure of nanomaterials generated by laser ablation in liquid solution?,” *Physical Chemistry Chemical Physics*, vol. 15, no. 9. pp. 3027–3046, Mar. 07, 2013. doi: 10.1039/c2cp42895d.

[33] G. Cao, *NANOSTRUCTURES AND NANOMATERIALS - Synthesis, Properties and Applications*. 2010. doi: 10.1142/9781860945960.

[34] H. Sadeghi, E. Solati, and D. Dorranian, “Producing graphene nanosheets by pulsed laser ablation: Effects of liquid environment,” *J Laser Appl*, vol. 31, no. 4, 2019, doi: 10.2351/1.5109424.

[35] P. P. Patil *et al.*, “Pulsed-laser--induced reactive quenching at liquid-solid interface: Aqueous oxidation of iron,” *Phys Rev Lett*, vol. 58, no. 3, pp. 238–241, Jan. 1987, doi: 10.1103/PhysRevLett.58.238.

[36] I. Y. Khairani, G. Mínguez-Vega, C. Doñate-Buendía, and B. Gökce, “Green nanoparticle synthesis at scale: a perspective on overcoming the limits of pulsed laser ablation in liquids for high-throughput production,” *Physical Chemistry Chemical Physics*, vol. 25, no. 29. Royal Society of Chemistry, pp. 19380–19408, Jul. 06, 2023. doi: 10.1039/d3cp01214j.

[37] G. W. Yang, “Laser ablation in liquids: Applications in the synthesis of nanocrystals,” *Progress in Materials Science*, vol. 52, no. 4. 2007. doi: 10.1016/j.pmatsci.2006.10.016.

[38] W. Nichols, T. Sasaki, and N. Koshizaki, “Laser ablation of a platinum target in water. III. Laser-induced reactions,” *J Appl Phys*, vol. 100, p. 114913, Dec. 2006, doi: 10.1063/1.2390642.

[39] W. T. "Nichols, T. "Sasaki, and N. [Nanoarchitectonics R. C. “Koshizaki National Institute of Advanced Industrial Science and Technology (AIST) Central 5 1-1-1 Higashi Tsukuba Ibaraki 305-8565 (Japan)],” “Laser ablation of a platinum target in water. II. Ablation rate and nanoparticle size distributions,” vol. 100, 2006, doi: https://doi.org/10.1063/1.2390641.

[40] R. Fabbro, J. Fournier, P. Ballard, D. Devaux, and J. Virmont, “Physical study of laser-produced plasma in confined geometry,” *J Appl Phys*, vol. 68, no. 2, 1990, doi: 10.1063/1.346783.

[41] C. Momma *et al.*, "Short-pulse laser ablation of solid targets," *Opt Commun*, vol. 129, no. 1–2, 1996, doi: 10.1016/0030-4018(96)00250-7.

[42] D. Perez, L. J. Lewis, P. Lorazo, and M. Meunier, "Ablation of molecular solids under nanosecond laser pulses: The role of inertial confinement," *Appl Phys Lett*, vol. 89, no. 14, 2006, doi: 10.1063/1.2358941.

[43] F. Mafuné, J. Y. Kohno, Y. Takeda, T. Kondow, and H. Sawabe, "Formation of gold nanoparticles by laser ablation in aqueous solution of surfactant," *Journal of Physical Chemistry B*, vol. 105, no. 22, 2001, doi: 10.1021/jp0037091.

[44] D. G. Shchukin and H. Möhwald, "Sonochemical nanosynthesis at the engineered interface of a cavitation microbubble," *Physical Chemistry Chemical Physics*, vol. 8, no. 30, 2006, doi: 10.1039/b606104d.

[45] T. Tsuji, Y. Tsuboi, N. Kitamura, and M. Tsuji, "Microsecond-resolved imaging of laser ablation at solid-liquid interface: Investigation of formation process of nano-size metal colloids," *Appl Surf Sci*, vol. 229, no. 1–4, 2004, doi: 10.1016/j.apsusc.2004.02.013.

[46] Z. Yan, R. Bao, Y. Huang, and D. B. Chrisey, "Hollow particles formed on laser-induced bubbles by excimer laser ablation of Al in liquid," *Journal of Physical Chemistry C*, vol. 114, no. 26, 2010, doi: 10.1021/jp104884x.

[47] W. Charee, V. Tangwarodomnukun, and C. Dumkum, "Laser ablation of silicon in water under different flow rates," *International Journal of Advanced Manufacturing Technology*, vol. 78, no. 1–4, 2015, doi: 10.1007/s00170-014-6625-6.

[48] G. K. Yogesh, S. Shukla, D. Sastikumar, and P. Koinkar, "Progress in pulsed laser ablation in liquid (PLAL) technique for the synthesis of carbon nanomaterials: a review," *Applied Physics A: Materials Science and Processing*, vol. 127, no. 11. Springer Science and Business Media Deutschland GmbH, Nov. 01, 2021. doi: 10.1007/s00339-021-04951-6.

[49] S. Barcikowski, A. Meńndez-Manjón, B. Chichkov, M. Brikas, and G. Račiukaitis, "Generation of nanoparticle colloids by picosecond and femtosecond laser ablations in liquid flow," *Appl Phys Lett*, vol. 91, no. 8, 2007, doi: 10.1063/1.2773937.

[50] A. Resano-Garcia *et al.*, "Highly-repeatable generation of very small nanoparticles by pulsed-laser ablation in liquids of a high-speed rotating target," *Physical Chemistry Chemical Physics*, vol. 18, no. 48, 2016, doi: 10.1039/c6cp06511b.

[51] P. Nandini, K. Akash, G. Rohit, S. Vipul, and I. A. Palani, "Investigations on the Influence of Liquid-Assisted Laser Ablation of NiTi Rotating Target to Improve the Formation Efficiency of Spherical Alloyed NiTi Nanoparticles," *J Mater Eng Perform*, vol. 26, no. 10, 2017, doi: 10.1007/s11665-017-2886-1.

[52] G. Marzun, A. Levish, V. Mackert, T. Kallio, S. Barcikowski, and P. Wagener, "Laser synthesis, structure and chemical properties of colloidal nickel-molybdenum nanoparticles for the substitution of noble metals in heterogeneous catalysis," *J Colloid Interface Sci*, vol. 489, 2017, doi: 10.1016/j.jcis.2016.09.014.

[53] B. Freeland *et al.*, "Real-time monitoring and control for high-efficiency autonomous laser fabrication of silicon nanoparticle colloids", doi: 10.1007/s00170-021-06772-6/Published.

[54] S. Kohsakowski *et al.*, "High productive and continuous nanoparticle fabrication by laser ablation of a wire-target in a liquid jet," *Appl Surf Sci*, vol. 403, 2017, doi: 10.1016/j.apsusc.2017.01.077.

[55] C. L. Sajti, R. Sattari, B. N. Chichkov, and S. Barcikowski, "Gram scale synthesis of pure ceramic nanoparticles by laser ablation in liquid," *Journal of Physical Chemistry C*, vol. 114, no. 6, 2010, doi: 10.1021/jp906960g.

[56] S. I. Kudryashov *et al.*, "High-throughput laser generation of Si-nanoparticle based surface coatings for antibacterial applications," *Appl Surf Sci*, vol. 470, 2019, doi: 10.1016/j.apsusc.2018.11.201.

[57] S. Dittrich, R. Streubel, C. McDonnell, H. P. Huber, S. Barcikowski, and B. Gökce, "Comparison of the productivity and ablation efficiency of different laser classes for laser ablation of gold in water and air," *Appl Phys A Mater Sci Process*, vol. 125, no. 6, 2019, doi: 10.1007/s00339-019-2704-8.

[58] H. Kobayashi, P. Chewchinda, H. Ohtani, O. Odawara, and H. Wada, "Effects of laser energy density on silicon nanoparticles produced using laser ablation in liquid," in *Journal of Physics: Conference Series*, 2013. doi: 10.1088/1742-6596/441/1/012035.

[59] P. Marabotti, S. Peggiani, A. Vidale, and C. Spartaco Casari, "Pulsed laser ablation in liquid of sp-carbon chains: Status and recent advances," *Chinese Physics B*, vol. 31, no. 12. 2022. doi: 10.1088/1674-1056/ac81b2.

[60] J. R. Heath, Q. Zhang, S. C. O'brien, R. F. Curl, H. W. Kroto, and R. E. Smalley, "The Formation of Long Carbon Chain Molecules during Laser

Vaporization of Graphite," *J Am Chem Soc*, vol. 109, no. 2, 1987, doi: 10.1021/ja00236a012.

[61] A. Wakisaka, J. J. Gaumet, Y. Shimizu, Y. Tamori, H. Sato, and K. Tokumaru, "Growth of carbon clusters. the simplest process, 2C1 → C2, observed via spectrometry and chemical reaction," *Journal of the Chemical Society, Faraday Transactions*, vol. 89, no. 7, 1993, doi: 10.1039/FT9938901001.

[62] J. J. Gaumet, A. El Ouachini, S. Peter, E. Millon, and J. F. Muller, "Formation of carbon clusters Cn ($1 \leq n \leq 4$) by laser vaporization of graphite and a study of their chemical reactivity by gas chromatography-mass spectrometry," *Journal of the Chemical Society - Faraday Transactions*, vol. 92, no. 11, 1996, doi: 10.1039/FT9969201831.

[63] M. Tsuji *et al.*, "Formation of hydrogen-capped polyynes by laser ablation of graphite particles suspended in solution," *Chem Phys Lett*, vol. 355, no. 1–2, 2002, doi: 10.1016/S0009-2614(02)00192-6.

[64] R. Matsutani, K. Inoue, N. Wad, and K. Kojima, "Wavelength dependence of polyyne preparation by liquid-phase laser ablation using pellet targets," *Chemical Communications*, vol. 47, no. 20, 2011, doi: 10.1039/c1cc00102g.

[65] M. Benoliel, "Investigation of naphthalene and its hydrogenated derivatives in the formation process of polyynes by Pulsed Laser Ablation in Liquid," 2019.

[66] M. J. Wesolowski, S. Kuzmin, B. Wales, J. H. Sanderson, and W. W. Duley, "Self-assembly of thin carbon micro-shells through pulsed laser irradiation of a ferrocene/benzene solution," *J Mater Sci*, vol. 48, no. 18, 2013, doi: 10.1007/s10853-013-7418-2.

[67] Y. E. Park, S. K. Shin, and S. M. Park, "The physical effects on the formation of polyynes by laser ablation," *Chem Phys Lett*, vol. 568–569, 2013, doi: 10.1016/j.cplett.2013.03.016.

[68] Y. E. Park, S. K. Shin, and S. M. Park, "Power dependence on formation of polyynes by laser ablation in water," *Bull Korean Chem Soc*, vol. 34, no. 4, 2013, doi: 10.5012/bkcs.2013.34.4.1039.

[69] A. Santagata *et al.*, "Carbon-based nanostructures obtained in water by ultrashort laser pulses," *Journal of Physical Chemistry C*, vol. 115, no. 12, 2011, doi: 10.1021/jp1094239.

[70] H. Tabata, M. Fujii, and S. Hayashi, “Synthesis of polyynes by laser ablation of diamond nanoparticles suspended in solution,” in *European Physical Journal D*, 2005. doi: 10.1140/epjd/e2005-00147-0.

[71] S. K. Shin, J. K. Song, and S. M. Park, “Preparation of polyynes by laser ablation of graphite in aqueous media,” in *Applied Surface Science*, 2011. doi: 10.1016/j.apsusc.2010.10.074.

[72] K. Inoue, R. Matsutani, T. Sanada, and K. Kojima, “Preparation of long-chain polyynes of C24H2 and C26H2 by liquid-phase laser ablation in decalin,” *Carbon*, vol. 48, no. 14. 2010. doi: 10.1016/j.carbon.2010.07.020.

[73] R. Matsutani, T. Kakimoto, K. Wada, T. Sanada, H. Tanaka, and K. Kojima, “Preparation of long-chain polyynes C18H2 and C20H2 by laser ablation of pellets of graphite and perylene derivative in liquid phase,” *Carbon*, vol. 46, no. 7. 2008. doi: 10.1016/j.carbon.2008.03.009.

[74] G. Compagnini, V. Mita, L. D’Urso, R. S. Cataliotti, and O. Puglisi, “Spectroscopic study of polyynes obtained by laser ablation in liquids,” in *Journal of Raman Spectroscopy*, 2008. doi: 10.1002/jrs.1837.

[75] G. Forte *et al.*, “The effects of liquid environments on the optical properties of linear carbon chains prepared by laser ablation generated plasmas,” in *Applied Surface Science*, 2013. doi: 10.1016/j.apsusc.2012.03.156.

[76] R. Matsutani, T. Kakimoto, H. Tanaka, and K. Kojima, “Preparation of polyynes by liquid-phase laser ablation using different irradiation target materials and solvents,” *Carbon N Y*, vol. 49, no. 1, 2011, doi: 10.1016/j.carbon.2010.08.044.

[77] Y. Park, S. K. Shin, and S. M. Park, “The solvent effects on the formation of polyynes by laser ablation,” *Bull Korean Chem Soc*, vol. 33, no. 7, 2012, doi: 10.5012/bkcs.2012.33.7.2439.

[78] Y. Wada, K. Koma, Y. Ohnishi, Y. Sasaki, and T. Wakabayashi, “Photoinduced reaction of methylpolyynes H(C≡C)nCH3 (n = 5-7) and polyyne H(C≡C)5H with I2 molecules,” *The European Physical Journal D*, vol. 66, no. 12, 2012, doi: 10.1140/epjd/e2012-30545-x.

[79] R. Paschotta, “Laser-induced Damage,” *RP Photonics Encyclopedia*. Feb. 29, 2024. doi: 10.61835/biw.

[80] R. Eastmond, T. R. Johnson, and D. R. M. Walton, “Silylation as a protective method for terminal alkynes in oxidative couplings: A general synthesis of the parent polyynes H(C⊚C)nH (n = 4–10, 12),”

Tetrahedron, vol. 28, no. 17, pp. 4601–4616, 1972, doi: https://doi.org/10.1016/0040-4020(72)80041-3.

List of Figures

List of Tables